energies

MDPI

Article

Optimal Allocation of Battery Energy Storage Systems to Enhance System Performance and Reliability in Unbalanced Distribution Networks

Dong Zhang [1,*], GM Shafiullah [1,*], Choton Kanti Das [2] and Kok Wai Wong [3]

[1] School of Engineering and Energy, College of Science, Technology, Engineering and Mathematics, Murdoch University, Perth, WA 6150, Australia
[2] School of Engineering, Edith Cowan University, Perth, WA 6027, Australia; choton46@gmail.com
[3] School of Information Technology, College of Science, Technology, Engineering and Mathematics, Murdoch University, Perth, WA 6150, Australia; k.wong@murdoch.edu.au
* Correspondence: 33759349@student.murdoch.edu.au (D.Z.); gm.shafiullah@murdoch.edu.au (G.S.)

Abstract: The continuously increasing renewable distributed generation (DG) penetration rate significantly reduces environmental pollution and power generation cost and satisfies society's rapid growth in electricity demand. Nevertheless, high penetration of renewable DGs, such as wind power and photovoltaics (PV), might deteriorate the system's efficiency and reliability due to its intermittent and stochastic natures. Introducing battery energy storage systems (BESSs) to the distribution system provides a practical method to compensate for the above deficiency since it can deliver and absorb power when needed. Hence, it is important to determine the optimal allocation of BESS to achieve maximum assistance in the grid. This study proposes an optimal BESS allocation methodology to improve reliability and economics in unbalanced distribution systems. The optimal BESS allocation problem is solved by simultaneously minimizing the cost of energy interruption, expected energy not supplied, power loss, line loading, voltage deviation, and BESS cost. The proposed technique is implemented and analyzed on a high renewable DG penetrated unbalanced IEEE-33 bus network using DIgSILENT PowerFactory software (version 2020 SP2A). An enhanced grey wolf optimization (EGWO) algorithm is developed to optimize BESS location and size according to the selected objective function. The simulation results show that the proposed optimal BESS optimization technique significantly improves the economics and reliability in unbalanced distribution systems and the EGWO outperforms the gray wolf optimization (GWO) and particle swarm optimization (PSO) algorithms.

Keywords: optimal allocation of BESS; reliability enhancement; DIgSILENT PowerFactory; line loading; voltage deviation; power loss minimization

Citation: Zhang, D.; Shafiullah, GM.; Das, C.K.; Wong, K.W. Optimal Allocation of Battery Energy Storage Systems to Enhance System Performance and Reliability in Unbalanced Distribution Networks. *Energies* **2023**, *16*, 7127. https://doi.org/10.3390/en16207127

Academic Editor: Carlos Miguel Costa

Received: 20 August 2023
Revised: 28 September 2023
Accepted: 14 October 2023
Published: 17 October 2023

1. Introduction

Due to the growing electricity consumption, expensive fossil fuels, and concerns about global warming, tons of renewable distributed generations (DGs), such as photovoltaic (PV) and wind generation, have been installed into the power network. Because renewable DGs usually emit negligible greenhouse gas and have lower electricity production costs than conventional power plants [1,2].

The main objective of the power system is to provide uninterrupted electricity to the consumer at a relatively lower cost. Therefore, economics and reliability are two fundamental characteristics of the power grid [3]. Many countries have integrated renewable DGs into their power grid to achieve this goal. The most recent research conducted by the international energy agency (IEA) forecasts that renewable electricity will increase 60% from the year 2020 to 2026, which is about 95% power capacity growth for the whole world [4]. The global power demand is continuously increasing because of the rapid rising in economic, population, and technological developments. Therefore, a reliable power supply is critical since social development mainly relies on electric power [5].

Reliability evaluation is considered as an essential basis for planning, operation, and designing of distribution networks. Almost 80% of power outages at the load level can be attributed to failures in distribution systems [6]. These power outages cause significant financial loss to the consumer, such as a reduction in production and sales, shortened lifespan of electrical equipment, and damage to raw materials because their various electrical equipment is sensitive to the change in power supply [7]. For reducing the financial loss caused by power outages, great importance is attached to system reliability enhancement in power sectors to minimize the duration and frequency of power unavailability for customers.

The conventional distribution system is radial, it only has a central power plant. When a failure or short circuit occurs in any grid branch, the fault must be eliminated to restore the power to that branch. This characteristic leads to a relatively low-reliability level for radial distribution systems because if faults happen in the main feeder, the system will stop supplying power to all downstream laterals [6]. Integrating renewable DGs into the load points is a key solution to overcome the above drawback since they can supply power to the consumer when faults occur in the grid.

Moreover, the utilization of renewable DGs, such as PV and wind generation, is a promising alternative for mitigating global warming and meeting the rapidly growing power demand of the world because of their inexhaustible and environment-friendly nature [8,9]. When introducing renewable DGs to the grid, they might introduce severe issues to the grid operation, for example the output power of this type of DG is highly random, which will magnify the volatility level of the power system. These issues will significantly deteriorate the system frequency and voltage, leading to worse economics and reliability of the grid [10]. Integrating BESS into the power system provides an effective solution to mitigate the negative impact of renewable DGs due to their fast power storing and delivering capability leading to a stabler grid frequency and voltage [1,11].

However, BESS has not been broadly applied to the grid mainly due to its high installation cost [12–18]. For example, in Western Australia's South-West Interconnected System (SWIS), the installation expense is generally higher than the profit the customer can receive during the BESS's lifespan [19]. Moreover, it does not guarantee system frequency and voltage improvement if the site and rating of BESS are randomly identified, deteriorating the system reliability and increasing the power loss and installation cost. Optimally allocating the BESS provides an effective solution to solve the above drawbacks, such as diminishing the time of overcharge can extend the lifespan of BESS [1,13,20,21]. Researchers have proposed several methodologies [16–18,20–37] to optimally place and size BESS to enhance the system's reliability and economics.

Ref. [34] proposes a simultaneous perturbation stochastic approximation method to optimally place and size BESS in an IEEE unbalanced 34 bus distribution system for system expenditure, including BESS cost and energy from the upstream system. Unfortunately, the model in [34] fails to consider system reliability in the total expenditure function. Ref. [22] improves the distribution system reliability by optimally placing the BESS on the grid through a two-stage model. Ref. [23] proposes a particle swarm optimization (PSO) algorithm that optimally allocates BESS into the distribution network for reliability enhancement. This study did not analyze system performance, such as voltage profile, line loading, and network losses. An optimal planning methodology is proposed in [38] for the coordinated allocation of DG and BESS in an active distribution network that significantly reduces the total investment and reliability cost of power utilities. In [24], an immune-genetic algorithm is proposed to enhance network reliability in the wind DGs penetrated IEEE balanced 33 bus radial distribution network. Nevertheless, the effectiveness of the proposed reliability enhancement technique on unbalanced power systems was not analyzed. The revenue of the power utilities is maximized in [21] by minimizing the power loss and installation expense of BESS and improving the voltage profile and lifespan of BESS. The same problem is also addressed in [25] through an equal-cost energy ratio method. Again in [18], the same objectives are accomplished through the coordinated

allocation of DG and BESS by employing the non-dominated sorting genetic algorithm-II (NSGA-II) approach combined with a utopian point method. Ref. [37] achieves optimal uniform BESS placement and sizing through PSO, subject to power loss, line loading, and voltage deviation reduction in unbalanced distribution systems, whereas the system reliability was not considered. In [26], mixed-integer convex programming is hybridized with PSO technique to minimize the power system cost by reducing power losses and voltage fluctuation. However, the suitability of the proposed methodology on other types of BESS except lithium-ion battery was not investigated. In [27], system efficiency are improved by minimizing the load interruption, total BESS cost, and power loss using a hybrid algorithm that combines PSO and genetic algorithm (GA). However, Ref. [27] only takes wind DG into account. Other renewable DGs can also be considered. In [20], minimization of annual cost and voltage fluctuation are accomplished in IEEE balanced 123 bus distribution system using a simulated annealing PSO algorithm. However, the impact of capacity optimization of BESS on power network economics was not investigated. In [28], the greedy algorithm by MATLAB is employed for optimally placing BESS into an IEEE 33 bus system to maximize the BESS's benefit. In [29], an improved immune genetic algorithm (IIGA) hybridized with the novel optimal affine power flow (OAPF) technique is used for optimally allocating BESS into a highly renewable DG penetrated distribution system. In this research, BESS installation cost and voltage fluctuation are minimized to satisfy the technical and economic requirements of the grid. In [16], optimal BESS allocation is achieved through a dynamic programming optimization approach to maximize the penetration rate of renewable DG and total investment cost. Coordinated allocation of renewable DG and BESS performed and validated through a multi-objective sensitivity analysis algorithm in [30] to improve the profit of the distribution company by minimizing the voltage deviation and investment cost of PV and batteries. Unfortunately, the algorithm applied in [28] lacks accuracy in finding the global optima. In [31], the placement and sizing of BESS are performed to maximize the economic, technical, and environmental benefits to the distribution system. The study employs a fuzzy-based extended version of NSGA II to find the optimal solution to the proposed objective function. Nevertheless, the proposed methodology is not applicable to large geographically spanned power networks since the authors assume solar radiation availability is the same on all nodes. In [17], an optimal BESS allocation methodology in an active distribution network is performed to minimize BESS installation cost, voltage deviations, line congestion, and power supply cost. Ref. [32] achieves optimal capacity configuration of BESS to minimize power flow fluctuation and improve the PV penetration rate to maximize the profit of consumers and power companies. An optimal planning approach for allocating BESSs in distribution networks is determined in [33], considering post-fault system reconfiguration. This study uses a stochastic planning algorithm and general algebraic modeling system software (a high-level system simulator) to minimize the annual network cost and voltage deviation cost. Ref. [35] mainly focus on the power system cost minimization, whereas costs of BESS and line loading are not covered in the objective function. In this study, a hybrid algorithm that combines Clayton Copula method, a point estimation technique, and PSO are used to optimally allocate BESS in a multi-correlated wind power distribution network. The methodology proposed in [36] addresses the optimal BESS sizing for reliability improvement in rural power networks through a Monte Carlo simulation-based algorithm.

To sum, despite noteworthy contributions in the knowledge domain, there are gaps that have not been investigated in the previous research, including:

- Reliability analysis has rarely been conducted in optimal BESS planning, particularly in unbalanced distribution systems. During the distribution system planning phase, it is significant to deliver relatively lower cost and minimal interrupted power to the customer [39].
- System performance indices, such as voltage deviation, line loading, and network losses, have not been considered altogether in previous literature except in [14,40]. However, these parameters are vital in managing the system's thermal and voltage stability.

- Almost all proposed models consider a balanced network, which is not practical. In the real world, system voltage is rarely balanced, mainly due to the unbalanced loading in the distribution system [41]. For instance, phase imbalance frequently occurs in US distribution systems, particularly the medium voltage level grid [42]. Severe voltage unbalance would magnify the system losses and shrink the capacity of the electrical components in the network [43]. Therefore, it is necessary to improve the reliability and economics of unbalanced distribution systems.

To solve these research gaps, an optimal BESS allocation methodology is proposed in this research to improve the system efficiency and reliability in unbalanced distribution networks. The enhanced grey wolf optimization (EGWO) is employed for optimization due to its robust global optima searching capability compared with other algorithms, such as PSO, grey wolf optimization (GWO), and GA [13,44]. EGWO is a more efficient variant of GWO that considers the distinct weights for leader wolves according to the leadership hierarchy, adaptively predicting the probable position of the prey, and mimicking the random walk behavior of the pack. GWO [45–48] and PSO algorithm [49,50] are utilized to verify the solutions generated from the EGWO. Furthermore, the Python programming language is employed to control the system model constructed in DIgSILENT PowerFactory software.

The remainder of this paper is structured in seven sections. The reliability indices used in this research are specified in Section 2. Section 3 describes the problem, which contains the proposed objective function and relevant constraints. The optimization methodology for solving the objective function is mentioned in Section 4. Section 5 introduces the testing system and the required indices for verifying the efficacy of the proposed approach. The effectiveness of the proposed model is verified through six case studies in Section 6. Finally, the conclusions are summarized in Section 7.

2. Reliability Assessment in the Distribution System

With the continuously increasing power demand, utilities need to conduct performance analysis to withstand the line congestion caused by growing demand and supply uninterrupted power to the consumer at a relatively lower cost. Power system reliability, which describes grids' ability to satisfy load demand at any time [51], is one of the key performance indicators. Currently, around 80% of power outages of the whole power system occur in distribution networks, which are directly connected to many consumers [7]. These power outages cause a significant financial loss to the consumer because their various electrical equipment is sensitive to the change in power supply. Therefore, it is essential to enhance the system's reliability by minimizing the duration and frequency of power unavailability for customers. Integrating BESS into the grid is one of the effective ways to improve system reliability. Because their fast power storing and delivering capability can mitigate the negative impact brought by renewable DGs. The performance metrics for assessing the effect of optimal BESS allocation on system reliability can be analyzed by expected energy not supplied (EENS) and expected interruption cost (EIC) [7,10]. These indices are described as follows:

2.1. Expected Energy Not Supplied

The reliability indices are derived from three basic reliability parameters, which are annual outage duration (T), average outage time (r), and average failure rate (λ), as presented in (1)–(3), respectively [52].

$$\lambda = \sum_i \lambda_i \tag{1}$$

$$T = \sum_i \lambda_i r_i \tag{2}$$

$$r = \frac{T}{\lambda} = \frac{\sum_i \lambda_i r_i}{\sum_i \lambda_i} \tag{3}$$

where λ_i and r_i are average failure rate and average outage time at load point i, respectively.

Expected energy not supplied (EENS) provided in (4) represents the expected amount of energy not delivered to the loads over a period when the power demand is larger than the available generation capacity [7,10,53]. It is one of the essential indexes for power companies to evaluate power system reliability. The amount of unmet electricity is usually measured in MWh over a year.

$$EENS = \sum_i L_i \cdot T_i \tag{4}$$

where L_i is the average load at load point i, as presented in (5) [23].

$$L_i = \frac{E_i^d}{t} \tag{5}$$

where E_i^d is the total energy demand of load i in the given period, t is the period of interest, usually one year.

2.2. Expected Interruption Cost

The expected interruption cost (EIC) provided in (6) indicates the cost of energy not supplied to the load because of the power outage [6,54]. It is measured in cost over a period usually defaulted as one year.

$$EIC = \sum_i L_i \cdot N_{c,i} \cdot f_i \cdot \lambda_i \tag{6}$$

where $N_{c,i}$ is the quantity of elements whose fault will cause interruption at load point i, f_i is the cost of interruption/composite customer damaged function.

2.3. Total Outage Cost

The summation of EIC and EENS, which is the total outage cost as presented in (7), can be applied to assess the reliability worth of the distribution network [6,7,54]. The cost of EENS can be calculated by multiplying a cost rate ε. In this research, ε is set to 20 USD/kWh [55].

$$TOC = \varepsilon \cdot EENS + EIC \tag{7}$$

2.4. Other Reliability Index

System average interruption duration index (SAIDI), a widely used reliability index as provided in (8) [56], is also considered in this research. This reliability index describes the level of impact caused by a number of disturbances to the customer at the load points, which is essential for evaluating the reliability of distribution systems.

$$SAIDI = \frac{\sum T_i \cdot N_i}{\sum N_i} \tag{8}$$

where N_i shows the number of customers at load point i.

3. Problem Formulation

3.1. Objective Function

This paper aims to enhance the system reliability and system performance and minimize the investment cost of BESS units by optimally placing and sizing BESS while satisfying the system constraints. The system performance cost consists of voltage deviation cost (VDC), power loss cost (PLC), and line loading cost (LLC), which are the critical parameters in distribution system planning. The objective function (9) is a cost function formulated by Equations (10)–(18) [7,13,54]. It comprises the cost of reliability (TOC), VDC, PLC, LLC, and cost of BESS units ($BESSC$), which are weighted equally with

λ_{REL}= λ_{VD} = λ_{PL} = λ_{LL} = λ_{BESS} = 1. (Where, λ_{REL}, λ_{VD}, λ_{PL}, λ_{LL}, and λ_{BESS} are weighting factors of *TOC*, *VDC*, *PLC*, *LLC*, and *BESSC*, respectively.)

$$F = min(\lambda_{REL} \cdot TOC + \lambda_{VD} \cdot VDC + \lambda_{PL} \cdot PLC + \lambda_{LL} \cdot LLC + \lambda_{BESS} \cdot BESSC) \quad (9)$$

where

$$VDC = \sum_{i=1}^{B} \frac{\left| V_{target} - V_{bm}(M_{m,size}, M_{m,site}) \right|}{V_{target}} \cdot \Delta t \cdot \delta_{VD} \quad (10)$$

$$PLC = \sqrt{\{P_{TLoss}(M_{m,size}, M_{m,site})\}^2 + \{Q_{TLoss}(M_{m,size}, M_{m,site})\}^2} \cdot \Delta t \cdot \delta_{loss} \quad (11)$$

$$P_{TLoss}(M_{m,size}, M_{m,site}) = \sum_{l=1}^{L} P_{Loss}(m,n) = \sum_{l=1}^{L} \left(R(m,n) \cdot \frac{P^2 + Q^2}{\left| \{V_{bm}(, M_{m,site})\}^2 \right|} \right) \quad (12)$$

$$Q_{TLoss}(M_{m,size}, M_{m,site}) = \sum_{l=1}^{L} Q_{Loss}(m,n) = \sum_{l=1}^{L} \left(X(m,n) \cdot \frac{P^2 + Q^2}{\left| \{V_{bm}(M_{m,size}, M_{m,site})\}^2 \right|} \right) \quad (13)$$

$$S_{TLoss}(M_{m,size}, M_{m,site}) = \sqrt{\{P_{TLoss}(M_{m,size}, M_{m,site})\}^2 + \{Q_{TLoss}(M_{m,size}, M_{m,site})\}^2} \quad (14)$$

$$LLC = \sum_{l=1}^{L} \%LL_{l,BESS} \cdot \Delta t \cdot \delta_{LL} \quad (15)$$

$$\%LL_{l,BESS} = \left(\frac{L^l_{BESS}}{L^l_{rated}} \right) \cdot 100 \quad (16)$$

$$BESSC = \sum_{i=1}^{K} M_{m,size} \cdot C_U \quad (17)$$

$$TOC = \sum_{i=1}^{B} \varepsilon \cdot EENS_i + EIC_i \quad (18)$$

The following values are considered in this study for analyses (in this study, a 2% annual increase rate is applied to δ_{loss}, δ_{VD}, and δ_{LL}, which are cost rates of power loss, voltage deviation, and line loading, respectively.): δ_{loss} = 0.287 USD/kWh [14], δ_{VD} = 0.163 USD/p.u./h [57], V_{target} = 1 p.u., δ_{LL} = 0.544 USD/p.u./h [14], C_U = 30,000 USD/MWh/year [58], and ε = 20 USD/kWh [55].

3.2. Objective Function Constraints

The multi-objective function (9) is subjected to the operational limits (19)–(26) and boundary conditions (27)–(33) for BESS modelling. Equations (19) and (20) indicate that real and reactive power always remains the same when boarding and leaving bus m. Equation (21) states the voltage magnitude constraint for bus m. Equations (22) and (23) denote the limits regarding BESS allocation. Equations (24)–(26) state the boundary limits for charging and discharging BESS [57].

$$P^{gen}_m + \sum_{n \epsilon N+} \left(P^{del}_{nm} \right) = P^{con}_m + \sum_{d \epsilon N-} \left(P^{del}_{md} \right) \quad (19)$$

$$Q^{gen}_m + \sum_{n \epsilon N+} \left(Q^{del}_{nm} \right) = Q^{con}_m + \sum_{d \epsilon N-} \left(Q^{del}_{md} \right) \quad (20)$$

$$V_{min} < \left| V^t_{bm} \right| < V_{max} \quad (21)$$

$$M_{m,site} = \begin{cases} 0, \ if \ the \ BESS \ is \ active \\ 1, \ otherwise \end{cases} \tag{22}$$

$$M_{m,size} = \begin{cases} Assign, \ if \ M_{m,site} = 0 \\ 0, \ if \ M_{m,site} = 1 \end{cases} \tag{23}$$

$$P_{min} < P_{BESS} < P_{max} \tag{24}$$

$$P_c^t \leq P_{BESS}^t \leq P_d^t \tag{25}$$

$$E_{min} < E_{BESS} < E_{max} \tag{26}$$

3.3. BESS Modelling

Currently, there are many types of batteries, including sodium-sulfur (NaS), lead-acid, lithium-ion, and flow batteries. The lithium-ion battery is the most prevalent type of battery, occupying 90% of the global battery market [59]. Compared with other battery storage types, the lithium-ion battery has a relatively high specific energy and power, high charge/discharge efficiency (80–90%) [60], and a low self-discharge rate. Moreover, its battery pack price has significantly dropped 73% from 2013 to 2018 [61], and the price will continuously decrease from USD176/kWh in 2018 to USD62/kWh in 2030, as predicted by Bloomberg New Energy Finance (BNEF) [59]. In the meanwhile, the performance of the lithium-ion battery has continuously improved. The latest research regarding lithium-ion batteries focused on replacing its anode material graphite with graphite/silicon (oxide) composites to improve the power density, making it a longer-term battery [62]. In the distribution system, lithium-ion batteries are mainly used to facilitate the penetration of renewable DGs. For example, Hornsdale Power Reserve installed the world's largest lithium-ion battery in the mid-north region of South Australia in 2017 to stabilize the intermittent power output of the Hornsdale Wind Farm [63]. Synergy also plans to build Western Australia's biggest lithium-ion battery by the end of 2022, which is about 100 MW/200 MWh at Kwinana Power Station, to deal with the rapid growing rooftop solar panels' installation [4]. Given the above considerations, a lithium-ion battery is chosen as the BESS type in this paper. The Equations (27)–(33) are used in this study to develop BESS model which is generic and can be applied to other BESS types also.

$$0.2 \leq S_{BESS}^k \leq 0.9 \tag{27}$$

$$P_c^t = max\left\{P_{min}, \frac{(E_t - M_{size,\,max})}{\eta_c \cdot \Delta t}\right\} \tag{28}$$

$$P_d^t = min\left\{P_{max}, \frac{(E_t - M_{size,min})\eta_d}{\Delta t}\right\} \tag{29}$$

$$E_{t+1} = min\left\{\left(E_t - \Delta t P_c^t \eta_c\right), \ M_{size,\,max}\right\} \tag{30}$$

$$P_c^t \leq P_{BESS}^t \leq P_d^t \tag{31}$$

$$E_{t+1} = max\left\{\left(E_t - \Delta t \frac{P_d^t}{\eta_d}\right), \ M_{size,\,min}\right\} \tag{32}$$

$$P_c^t \leq P_{BESS}^t \leq P_d^t \tag{33}$$

The state of charge of BESS (S^k_{BESS}) is subjected to constraints (27). (S^k_{BESS}) = 1 represents that the BESS is fully charged. And BESS is discharged up to 20% if (S^k_{BESS}) = 0.2. Equations (28) and (29) generate the charging and discharging rate for BESS, respectively [64]. Constraint (30) calculates the amount of energy stored in the BESS in charging mode, and constraint (31) restricts the charging power of BESS. Correspondingly, the energy released from the BESS is calculated by (32) in discharging mode, and (33) sets the limits for discharging power of BESS.

4. Optimization Algorithm

4.1. EGWO Approach

This paper adopts the EGWO algorithm proposed in [65] to handle the BESS allocation problem to minimize the performance cost and enhance the distribution system's reliability. The EGWO is an upgraded version of the popular meta-heuristic optimization algorithm, GWO. The GWO emulates the social structure and hunting strategies of grey wolf packs to find the global optimum of the problem [66]. In the mathematical framework of the GWO algorithm, each grey wolf symbolizes a potential solution. The wolf with the best fitness value is designated as the α wolf, while the second and third best are β and δ wolves, respectively. All other wolves in the population are treated as ω wolves, which adjust their position by following the guidance of the top three wolves. After each adjustment, the pack recalculates its fitness. The three best-performing wolves are automatically promoted to the roles of α, β, and δ wolves. This iterative process ensures a gradual approach towards the optimal solution, eventually identifying the α wolf as the best solution.

To improve the convergence speed and quality of the solution generated by the traditional GWO technique, the EGWO presents a more efficient variant by considering the distinct weights for leader wolves according to the leadership hierarchy, adaptively predicting the probable position of the prey, and mimicking the random walk behavior of the pack, which are delineated by (35), (34), and (38), respectively [65]. The flowchart of the EGWO algorithm is illustrated in Figure 1.

In EGWO, the position of the prey is dynamically determined through a weight-based Equation (34).

$$x^j_p(t) = \delta_\alpha \cdot x^j_\alpha(t) + \delta_\beta \cdot x^j_\beta(t) + \delta_\gamma \cdot x^j_\gamma(t) + \varepsilon(t) \tag{34}$$

where, j and t correspondingly represent the current dimension and iteration of the problem. δ_α, δ_β, and δ_γ, satisfying conditions (35) and (36), are weighting factors of α, β, and δ wolves, respectively. $\varepsilon(t)$ represents a simulated stochastic error, conforming to the Gaussian distribution with a mean value of 0 and standard deviation $\sigma(t)$. The characteristic of $\sigma(t)$ is defined by (37).

$$1 \geq \delta_\alpha > \delta_\beta > \delta_\gamma \geq 0 \tag{35}$$

$$\delta_\alpha + \delta_\beta + \delta_\gamma = 1 \tag{36}$$

$$\sigma(t) > \sigma(t+1) \tag{37}$$

Under the guidance of α, β, and δ wolves, the position of each wolf i is navigated directly towards the predicted location of the prey, as expressed by the subsequent Equation (38).

$$x^j_i(t+1) = x^j_p(t) - \varphi \cdot \left| x^j_p(t) - x^j_i(t) \right| \tag{38}$$

where φ represents a random number selected from the interval [–2, 2].

When the wolf position determined by Equation (38) goes beyond the predefined boundaries, it will be rectified by executing a random move towards the boundary, according to (39).

$$x^j_i(t+1) = \begin{cases} x^j_i(t) + \gamma \cdot \left(ub^j - x^j_i(t) \right), \ if \ x^j_i(t+1) > ub^j \\ x^j_i(t) + \gamma \cdot \left(lb^j - x^j_i(t) \right), \ if \ x^j_i(t+1) < lb^j \end{cases} \tag{39}$$

where, ub^j and lb^j respectively denote the upper and lower boundaries for jth dimension. γ is a random number in the range [0, 1].

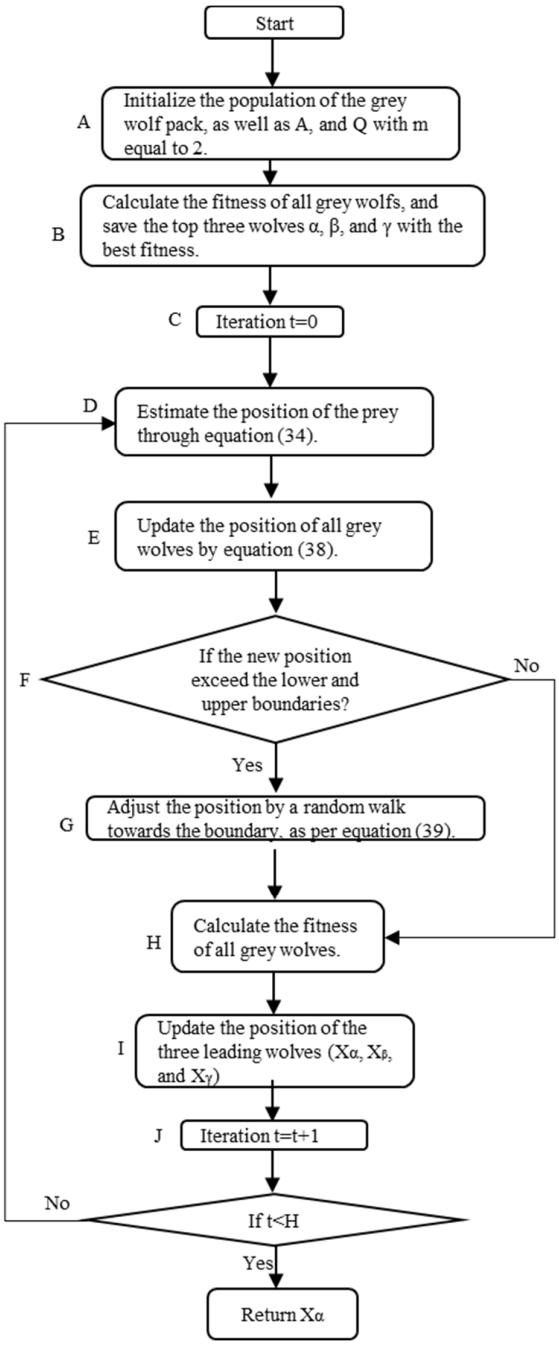

Figure 1. Flowchart of EGWO algorithm.

4.2. Proposed Methodology

Figure 2 illustrates the proposed BESS allocation strategy using the EGWO approach. After inputting the essential data into all grid components, EGWO parameters are initialized. The parameters and variables utilized in the optimization process are tabulated in Table 1. Scaling factor for time variant load and DGs were adopted from Ref. [57] and applied to loads and DGs in the test system. Voltage dependency is created for scaling feeder loads. Next, the optimal BESS placing and sizing problem is created to minimize the total cost, including TOC, VDC, PLC, LLC, and BESSC. There are two categories for BESS sizing: (1) using uniform BESS size; (2) using non-uniform BESS size.

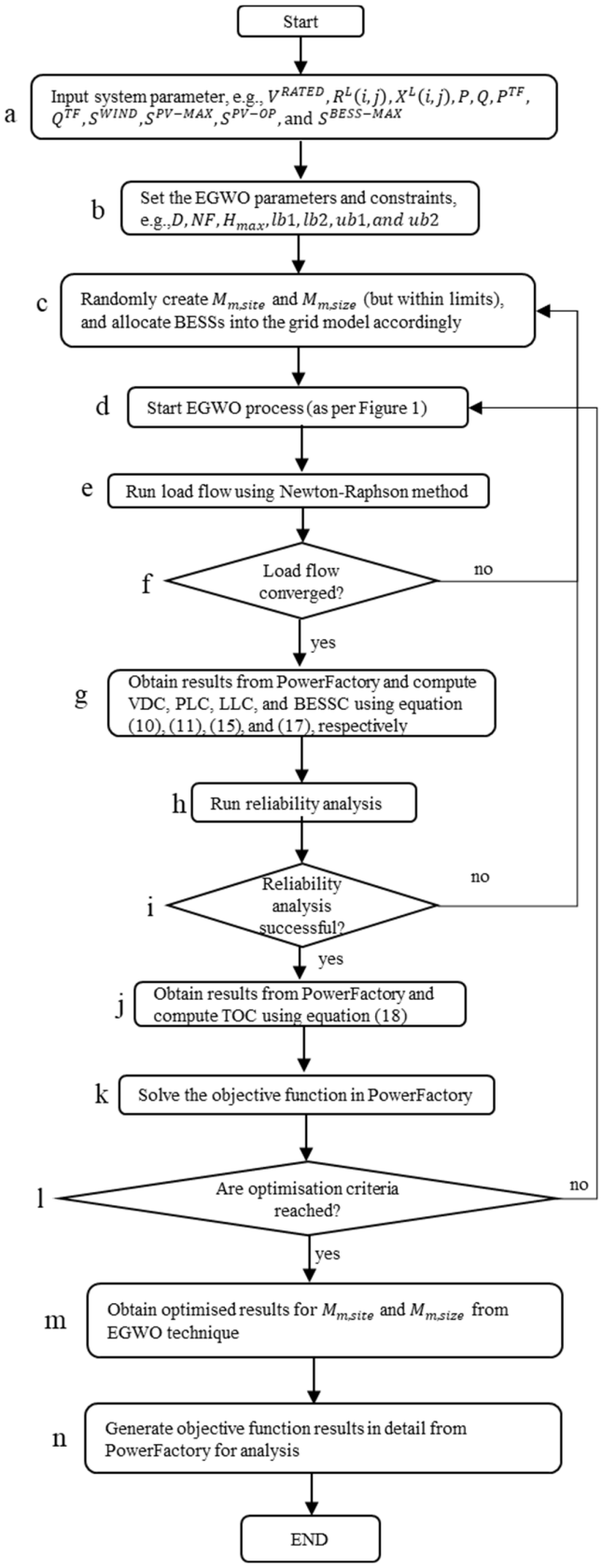

Figure 2. Proposed BESS allocation methodology with EGWO algorithm.

Table 1. EGWO parameters and variables.

Type	Parameters/Variables	Description/Settings
Input parameters	$V^{Rated}, R(m,n), X(m,n), P, Q, P^{TF}, Q^{TF}, S^{Wind}, S^{PV-Max}, S^{PV-OP}$, and $S^{BESS-Max}$	Critical for the distribution system model
Output parameters	TOC, VDC, PLC, LLC, and BESSC	Critical for the objective function
Decision variables	$M_{m,size}$	Determine the sizes of BESSs in MVA with a unity power factor.
	$M_{m,site}$	Determine the locations of BESSs in the grid.
EGWO parameters	φ, γ	Settings: $\varphi \in [-2, 2]$, $\gamma \in [0, 1]$
	D, NF, H_{max}	Settings: $D = 2, NF =$ population size $= 80$, $H_{max} =$ maximum iteration $= 1000$
EGWO bounds	For $M_{m,site}$: lb1, and ub1	Settings: lb1 = 0.1 MVA and ub1 = 2 MVA
	For $M_{m,size}$: lb2, and ub2	Settings: lb2 = 0 and ub2 = 1

The position of BESS is determined by the decision variable $M_{m,site}$, where $M_{m,site} = 0$ states that a BESS at bus m is active and $M_{m,site} = 1$ represents that the BESS at bus m is inactive. The sizes of BESSs, $M_{m,size}$, distributed in the grid are generated randomly within the limit of 0.1 MVA to 2 MVA. The determination of BESS sizes is subject to the lower boundary (lb1) and upper boundary (ub1) of $M_{m,site}$, lower boundary (lb2) and upper boundary (ub2) of $M_{m,size}$, string size of BESS, bus size, transformer size, and inverter specifications. In the end, the optimized results of $M_{m,size}$ and $M_{m,site}$ are generated through the EGWO process under the objective function constraints to supply desired MW to improve the system reliability and power quality and minimize system losses, line loading, and investment for BESS units.

5. Testing Network and System Performance Indices

This section introduces the testing system for verifying the efficacy of the proposed methodology, assignment of factors for scaling the feeder and forming voltage dependence of loads, and the required indices for evaluating system performance and reliability improvement.

5.1. Test System

The proposed methodology is tested in a modified IEEE 33 bus system with high renewable penetration, as shown in Figure 3. DIgSILENT PowerFactory software is employed for building the system model. In the test system, three 400 kVA solar DGs are connected at Bus05, Bus21, and Bus31; four 500 kVA solar DGs are allocated to Bus08, Bus12, Bus28, and Bus33; and two 1 MW wind DGs are installed on Bus18 and Bus24. The wind and solar DGs and loads are modelled using built-in templates in PowerFactory. For the balanced 33-bus system, the network data for feeders and loads are listed in Appendix A Table A1. The unbalanced 33-bus system is originated from the above balanced system [67] by randomly distributing the load among three phases and maintaining the total load for each bus unchanged. The feeder and modified load data for the unbalanced system are presented in Appendix A Tables A1 and A2, respectively [68]. The base MVA and the substation voltage are 10 MVA and 12.66 kV, respectively. The voltage violation limits are assumed as ±6% [69]. All lines' outage rates and time are set as 0.035 fail/year and 18 h [22], respectively. The cost rate for energy not supplied is 20 USD/kWh [54,55]. The power flow equations used in this research are detailed in [70] and are addressed with the unbalanced three-phase Newton–Raphson approach.

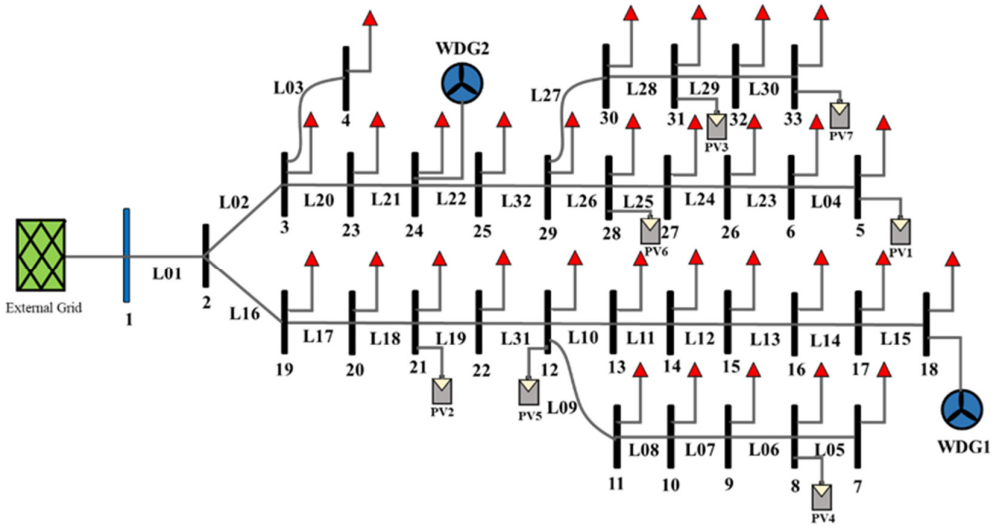

Figure 3. Proposed 33-bus distribution system model.

5.2. Feeder Scaling and Voltage Dependency

The test system load follows the IEEE-RTS model, and the feeder loads are scaled through the procedures mentioned in [14]. The total real and reactive power is calculated by employing a scale (Ψ^{SCALE}) and the load voltage dependency as shown in (40) and (41), respectively [14].

$$P = \Psi^{SCALE} \cdot P_0 \left[aP \cdot \left(\frac{V_{bm}}{V^{REF}} \right)^{e_{aP}} + bP \cdot \left(\frac{V_{bm}}{V^{REF}} \right)^{e_{aP}} + (1 - aP - bP) \cdot \left(\frac{V_{bm}}{V^{REF}} \right)^{e_{cP}} \right] \quad (40)$$

$$Q = \Psi^{SCALE} \cdot Q_0 \left[aQ \cdot \left(\frac{V_{bm}}{V^{REF}} \right)^{e_{aP}} + bQ \cdot \left(\frac{V_{bm}}{V^{REF}} \right)^{e_{aQ}} + (1 - aQ - bQ) \cdot \left(\frac{V_{bm}}{V^{REF}} \right)^{e_{cQ}} \right] \quad (41)$$

where, the load coefficients are set as $aP = aQ = 0.4$, $bP = bQ = 0.3$, and $cP = cQ = 0.3$, and the exponents are $e_{aP} = e_{aQ} = 0$, $e_{bP} = e_{bQ} = 1$, and $e_{cP} = e_{cQ} = 2$, and $cP = cQ = 0.3$ [14].

5.3. Indices for Evaluating System Performance Improvement

5.3.1. Indices for Voltage Deviation and Profile Improvement

V_{max} *and* V_{min} for mth bus are calculated by applying the ±6% voltage violation limits. The voltage deviation index is formulated as a percentage (%VDI), as shown in (42) [14].

$$\%VDI = \sum_{m=1}^{B} \left(\frac{|V^{RATED} - V_{bm}|}{V^{RATED}} \right) \cdot 100 \quad (42)$$

The voltage profile of mth bus (VP_m), overall voltage profile (VP), and voltage profile improvement index are expressed as (43)–(45), respectively [14], where $\sum_{m=1}^{B} \eth_m = 1$.

$$VP_m = V_{bm} M_{Lm} \eth_m \quad (43)$$

$$VP = \sum_{m=1}^{B} VP_m \quad (44)$$

$$VPII = \frac{VP_{with-ESS}}{VP_{no-ESS}} \quad (45)$$

5.3.2. Line Loading Index

The line loading index (LLI) denotes the grid's total line loading or demand level. The percentage line loading index ($\%LLI$) and percentage line loading of lth line for the base

scenario without BESS allocation and the scenario with BESS allocation are demarcated by (46), (47), and (16), respectively [14].

$$\%LLI = \frac{\%LLT_{with-ESS}}{\%LLT_{no-ESS}} \cdot 100 = \frac{\sum_{l=1}^{M} \%LL_{l,ESS}}{\sum_{l=1}^{M} \%LL_{l,BASE}} \cdot 100 \quad (46)$$

$$\%LL_{l,BASE} = \left(\frac{SL_{l,BASE}}{SL_{l,RATED}} \right) \cdot 100 \quad (47)$$

5.3.3. Power Loss Reduction Indices

The real ($PLsRI^P$), reactive ($PLsRI^Q$), and total line loss ($PLsRI^T$) of the grid are formulated by (48)–(50), respectively [14].

$$PLsRI^P = \frac{\sum_{l=1}^{M} P_{l,Ls-ESS}}{\sum_{l=1}^{M} P_{l,Ls-BASE}} \quad (48)$$

$$PLsRI^Q = \frac{\sum_{l=1}^{M} Q_{l,Ls-ESS}}{\sum_{l=1}^{M} Q_{l,Ls-BASE}} \quad (49)$$

$$PLsRI^T = \frac{\sum_{l=1}^{M} \sqrt{\left(P_{l,Ls-ESS}\right)^2 + \left(Q_{l,Ls-ESS}\right)^2}}{\sum_{l=1}^{M} \sqrt{\left(P_{l,Ls-BASE}\right)^2 + \left(Q_{l,Ls-BASE}\right)^2}} \quad (50)$$

5.3.4. Reliability Indices

The total outage cost reduction index (TOCRI) is calculated by (51).

$$TOCRI = \frac{\sum_{m=1}^{B} TOC_{m,with-ESS}}{\sum_{m=1}^{B} TOC_{m,no-ESS}} \quad (51)$$

where i is the load point number.

6. Results and Analysis

This section explores the benefit of optimal BESS allocation in reliability enhancement, cost of BESS minimization, voltage deviation, power loss, and line loading reduction in the distribution system. The simulation study is implemented in the DIgSILENT PowerFactory software version 2020 on a computer with Windows 10 64-bit, Intel(R) Xeon(R) 3.5 GHz processor, and 16 GB RAM. System performance is investigated and analyzed in six case studies, as shown below:

Case 1: no BESS allocation in the balanced 33-bus system.

Case 2a: uniform BESS allocation in the balanced 33-bus system with $\lambda_{VD} = \lambda_{PL} = \lambda_{LL} = \lambda_{BESS} = \lambda_{REL} = 1$ (All metrics are with the same weight of 1).

Case 2b: uniform BESS allocation in the balanced 33-bus system with $\lambda_{VD} = \lambda_{PL} = \lambda_{LL} = \lambda_{BESS} = 1$ and $\lambda_{REL} = 10$ (All metrics are with the same weight of 1 except λ_{REL} which is 10).

Case 3a: non-uniform BESS allocation in the balanced 33-bus system with $\lambda_{VD} = \lambda_{PL} = \lambda_{LL} = \lambda_{BESS} = \lambda_{REL} = 1$.

Case 3b: non-uniform BESS allocation in the balanced 33-bus system with $\lambda_{VD} = \lambda_{PL} = \lambda_{LL} = \lambda_{BESS} = 1$ and $\lambda_{REL} = 10$.

Case 4: no BESS allocation in the unbalanced 33-bus system.

Case 5a: uniform BESS allocation in the unbalanced 33-bus system with $\lambda_{VD} = \lambda_{PL} = \lambda_{LL} = \lambda_{BESS} = \lambda_{REL} = 1$.

Case 5b: uniform BESS allocation in the unbalanced 33-bus system with $\lambda_{VD} = \lambda_{PL} = \lambda_{LL} = \lambda_{BESS} = 1$ and $\lambda_{REL} = 10$.

Case 6a: non-uniform BESS allocation in the unbalanced 33-bus system with $\lambda_{VD} = \lambda_{PL} = \lambda_{LL} = \lambda_{BESS} = \lambda_{REL} = 1$.

Case 6b: non-uniform BESS allocation in the unbalanced 33-bus system with $\lambda_{VD} = \lambda_{PL} = \lambda_{LL} = \lambda_{BESS} = 1$ and $\lambda_{REL} = 10$.

To investigate and analyze the system performance in balanced and unbalanced distribution systems, Cases 1–3 are categorized as investigation category I (optimal BESS allocation in the balanced distribution system); Cases 4–6 are categorized as investigation category II (optimal BESS allocation in the unbalanced distribution system). To analyze the difference between uniform size BESS and non-uniform size BESS allocation, each investigation category has one case with uniform size BESS and one case with non-uniform BESS. Moreover, the weighting factor of system reliability, λ_{REL}, is changed from 1 (Case 2a, 3a, 5a, and 6a) to 10 (Case 2b, 3b, 5b, and 6b), aiming for better optimization results.

As mentioned earlier, EGWO was used to identify BESS's optimum location and size. The output of EGWO on BESS size and location is used for the optimization analysis conducted in this section. Moreover, the solutions generated from EGWO are compared with both GWO and PSO approaches to verify its efficacy.

6.1. Case 1 and 4—Case without BESS Allocation in the Balanced and Unbalanced Distribution System

For base Cases 1 and 4, the results of performance indices, including %VDI, %LLI, S_{TLoss}, and TOC (as per Equations (14), (18), (42) and (46)) listed in Table 2 represent the parameters desired to be optimized. The smaller the parameter results, the better the system performance. Although all these parameters are within the system constraints, there is space for further improvement.

Table 2. System results for various cases.

Case Studies	Apparent Power per BESS (MVA) and Their Sites	VDI (%)	LLI (%)	S_{TLoss} (MVA)	TOC (USD/Year)	Total BESS Size (MWh)	Objective Function Value (USD/Year)
Case 1:	No BESS	100.813	256.192	0.214	407,860	–	959,529.845
Case 2a:	BESS03, BESS06, BESS07, BESS08, BESS10, BESS11, BESS24, BESS27, BESS28, BESS30, BESS31, BESS32, BESS33, MVA for each BESS = 0.118	59.637	218.294	0.156	327,352	1.53	777,590.108
Case 2b:	BESS03, BESS06, BESS07, BESS11, BESS12, BESS13, BESS14, BESS17, BESS19, BESS22, BESS23, BESS24, BESS32, BESS33, MVA for each BESS = 0.184	40.834	231.279	0.174	301,029	2.571	832,955.828
Case 3a:	BESS03 = 0.154, BESS06 = 0.140, BESS07 = 0.212, BESS10 = 0.101, BESS12 = 0.221, BESS15 = 0.123, BESS16 = 0.141, BESS20 = 0.102, BESS21 = 0.228, BESS32 = 0.117, BESS33 = 0.123	63.918	217.094	0.16	343,117	1.662	807,263.689
Case 3b:	BESS03 = 0.113, BESS06 = 0.148, BESS07 = 0.221, BESS10 = 0.153, BESS11 = 0.144, BESS18 = 0.445, BESS21 = 0.1, BESS25 = 0.251, BESS26 = 0.262, BESS27 = 0.105, BESS28 = 0.149, BESS30 = 0.202, BESS32 = 0.111, BESS33 = 0.132	40.646	232.682	0.177	309,181	2.535	845,109.939
Case 4:	No BESS	100.993	309.421	0.220	445,480	–	1,014,773.731
Case 5a:	BESS05, BESS06, BESS07, BESS08, BESS09, BESS18, BESS24, BESS25, BESS26, BESS29, BESS30, BESS31, BESS32, BESS33, MVA for each BESS = 0.112	69.589	265.765	0.163	331,112	1.573	801,296.52

Table 2. *Cont.*

Case Studies	Apparent Power per BESS (MVA) and Their Sites	VDI (%)	LLI (%)	S_{TLoss} (MVA)	TOC (USD/Year)	Total BESS Size (MWh)	Objective Function Value (USD/Year)
Case 5b:	BESS03, BESS04, BESS06, BESS07, BESS08, BESS09, BESS14, BESS16, BESS18, BESS19, BESS20, BESS21, BESS30, BESS31, BESS32, BESS33, MVA for each BESS = 0.172	23.312	291.633	0.194	308,901	2.749	8,941,82.058
Case 6a:	BESS02 = 0.127, BESS03 = 0.161, BESS06 = 0.232, BESS08 = 0.131, BESS10 = 0.159, BESS11 = 0.140, BESS17 = 0.158, BESS28 = 0.232, BESS29 = 0.108, BESS32 = 0.115, BESS33 = 0.157	67.519	266.914	0.176	355,030	1.72	863,067.735
Case 6b:	BESS02 = 0.151, BESS05 = 0.183, BESS06 = 0.332, BESS08 = 0.241, BESS10 = 0.237, BESS11 = 0.221, BESS21 = 0.119, BESS22 = 0.1, BESS25 = 0.138, BESS26 = 0.126, BESS27 = 0.117, BESS29 = 0.142, BESS30 = 0.159, BESS31 = 0.218, BESS32 = 0.162, BESS33 = 0.233	27.321	291.213	0.209	319,687	2.881	945,827.482

6.2. Case 2 and 5—Uniform BESS Allocation in the Balanced (Case 2) and Unbalanced (Case 5) Distribution System

Optimal BESS allocation results through both uniform and non-uniform sizing approaches are displayed in Table 2. As mentioned earlier, the $M_{m,site}$ and $M_{m,size}$ was identified through the EGWO approach and shown in Table 2 by the BESS number and BESS MVA, respectively. For example, BESS24 = 0.118 represents a BESS of 0.118 MVA installed at bus 24. Thirteen 0.118 MVA BESSs and fourteen 0.184 MVA BESSs are allocated for Case 2a and Case 2b, respectively. It can be seen that all performance indices (%*VDI*, %*LLI*, S_{TLoss}, and *TOC*) in both Case 2a and Case 2b are decreased compared with Case 1. Although Case 2b, which provides more importance to *TOC* than other indices, achieves better system reliability (*TOC*)and voltage profile (%*VDI*) compared with Case 2a. However, it requires a larger total BESS size in Case 2b (2.571 MWh) than in Case 2a (1.53 MWh), which leads to a higher line loading (%*LLI*), power loss (S_{TLoss}), and a more significant distribution system investment cost. Therefore, Case 2a is the desired optimal solution for uniform size BESS allocation in the balanced distribution system considering system performance and investment cost. Similar results can also be found in uniform size BESS allocation in the unbalanced system (Case 5), that all performance indices (%*VDI*, %*LLI*, S_{TLoss}, and *TOC*) in Case 5a and Case 5b are lower than in Case 4. And Case 5a is more cost-effective compared with Case 5b.

6.3. Case 3 and 6—Non-Uniform BESS Allocation in the Balanced (Case 3) and Unbalanced Distribution System (Case 6)

The impact of non-uniform size BESS allocation in the balanced system is analyzed, and the outcomes are presented in Table 2. In this case, $M_{m,size}$ is assigned non-uniformly into the grid. Case 3b has a larger weighting factor of C_{REL} for achieving a better optimization outcome. It is apparent that all performance indices (%*VDI*, %*LLI*, S_{TLoss}, and *TOC*) in both Case 3a and Case 3b are decreased compared with Case 1. In contrast to Case 2a, %*LLI* in Case 3a is further minimized. But the required total BESS size is larger than Case 2a, which would cause an increase in distribution system investment cost. After giving more significance to *TOC* of Case 3b, *TOC* and %*VDI* are further reduced compared with Case 3a, while the total BESS size is improved. Similar results can also be found in non-uniform size BESS allocation in the unbalanced system (Case 6) that *TOC* and %*VDI* in Case 6b are decreased compared with Case 6a, while the total BESS size is further increased.

6.4. Results Analysis and Comparison

6.4.1. Voltage Profile

The bus voltage for individual bus numbers is displayed in Figures 4 and 5. Regarding investigation category I (Figure 4), bus voltages for almost all buses have been improved in both Cases 2 and 3 compared with Case 1. Case 2b achieves the best voltage profile among all cases. In this case, most bus voltages are near the rated voltage of 1 p.u. However, the voltage deviation at buses 10–18 and 20–22 is higher compared with Case 3b. Overall, Cases 2 and 3 achieve a better voltage profile than Case 1, where the voltage profile of Case 2a (%*VDI* = 59.637) is better than Case 3a (%*VDI* = 63.918). Similar to investigation category I (Figure 4), voltage profiles for all cases with BESS allocation in investigation category II (Figure 5) are significantly improved compared with Case 4. Case 5b provides the best voltage profile for most buses except buses 5, 6, 26, and 27, which are slightly worse than Case 6b. On the whole, cases with more significance to *TOC* (Case 2b, 3b, 5b, and 6b) provide a better voltage profile than cases with the same weighting factor (Case 2a, 3a, 5a, and 6a), as presented in Table 2.

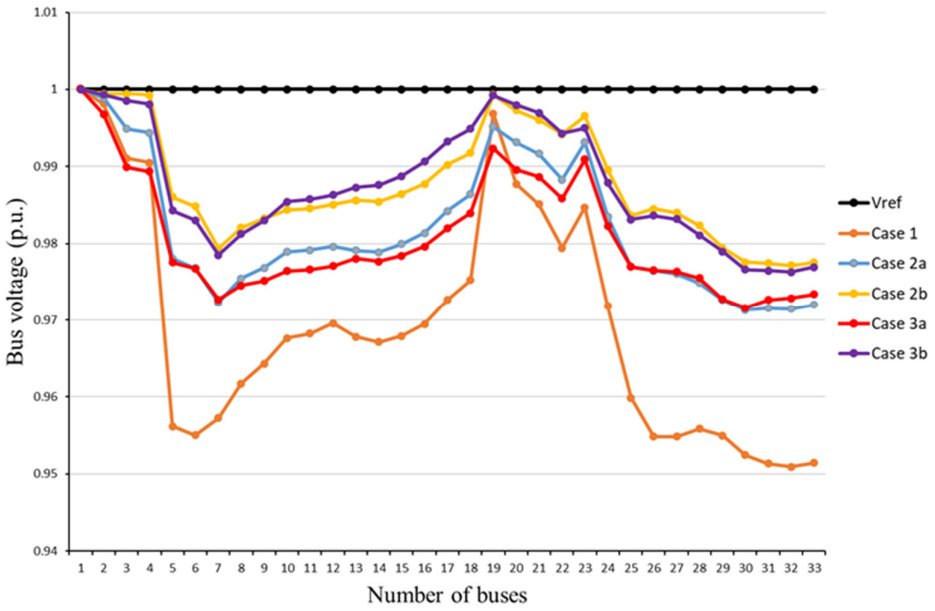

Figure 4. Voltage profile for investigation category I.

6.4.2. System Reliability Cost

The system reliability in both investigation categories is measured to evaluate the effects of integrating BESS for reliability improvement, as displayed in Figures 6 and 7. Both investigation categories have similar patterns, where *TOC*, *EIC*, cost of *EENS*, and *SAIDI* have the highest value for their base case. In addition, these reliability parameters are further reduced in cases with $\lambda_{REL} = 10$ (Cases 2b, 3b, 5b, and 6b) compared with the cases with $\lambda_{REL} = 1$ (Cases 2a, 3a, 5a, and 6a) since more importance is given to the system's reliability. *TOC*, *EIC*, and cost of *EENS* for all cases are illustrated in Figure 6, where the lowest costs are observed at Case 2b (*EIC* = 151,056 USD/year, cost of *EENS* = 149,834 USD/year, *TOC* = 301,029 USD/year) and Case 5b (*EIC* = 155,509 USD/year, cost of *EENS* = 153,540 USD/year, *TOC* = 308,901 USD/year) for investigation categories I and II, respectively.

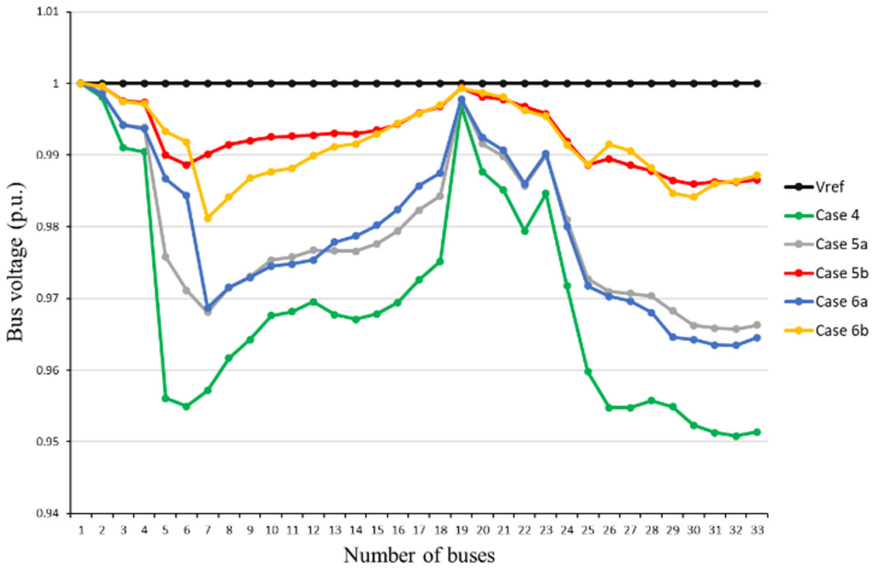

Figure 5. Voltage profile for investigation category II.

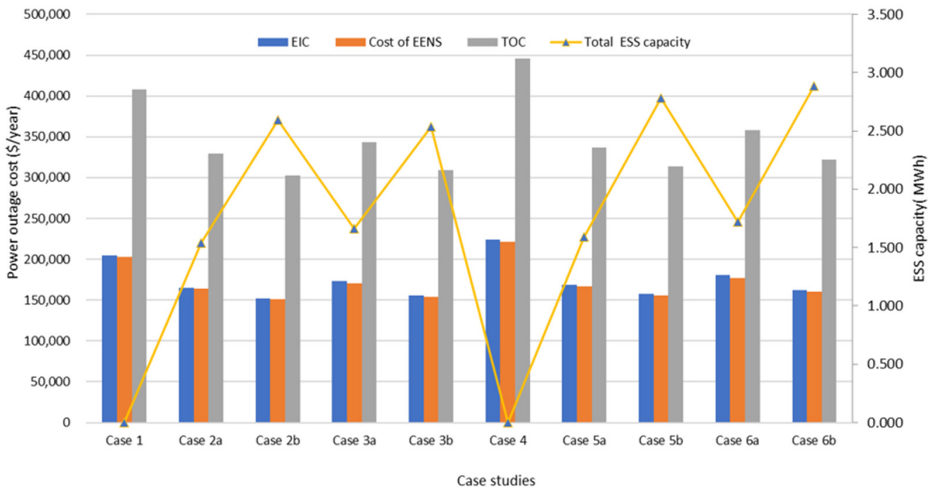

Figure 6. TOC, EIC, and EEENS costs for all cases.

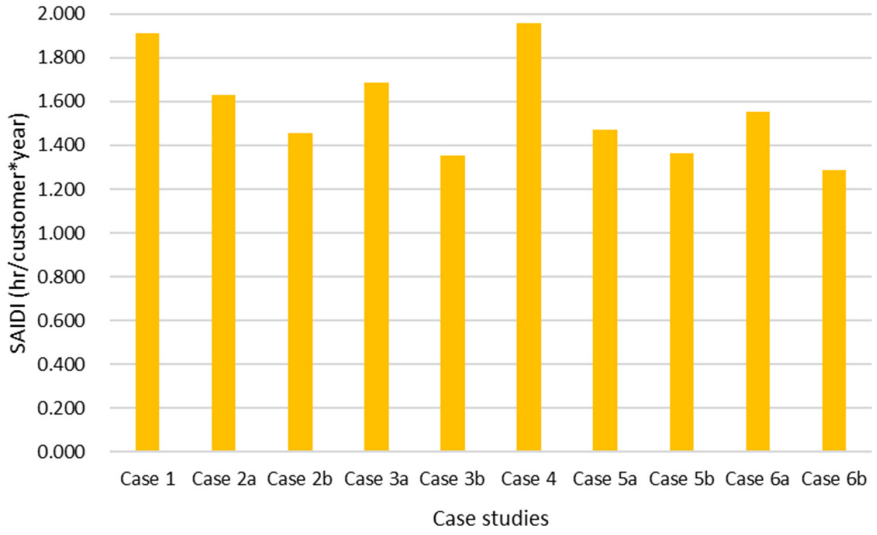

Figure 7. SAIDI for all cases.

Similar characteristics can also be noticed in the outcome of *SAIDI*, as exhibited in Figure 7. The results suggest that Case 3b (*SAIDI* = 1.353 h/customer × year) and Case 6b (*SAIDI* = 1.287 h/customer × year) improve the system reliability better than other options in investigation categories I and II while demanding more BESS installation.

Overall, it can be established that renewable DGs penetrated distribution systems without BESS allocation will magnify the frequency and duration of the power outage experienced by the consumers. In contrast, increasing the BESS capacity of optimal BESS planning in the distribution system can significantly increase the system's reliability and lower the *TOC* for consumers. This result substantiates the finding proposed in [7] that introducing BESS to renewable DG penetrated distribution systems can improve system reliability, such as reduced *TOC*, *EIC*, and cost of *EENS*, and *SAIDI*.

6.4.3. Line Loading and Line Losses

The performance comparison regarding line loading is depicted in Figures 8 and 9. All line loadings are within the constraint of 0 to 80%. According to Figure 8, L1 has the maximum loading among all cases (36.614% for the base case and around 29% for Cases 2 and 3). L2 has a load of 24.606% for the base case and around 20% for the other cases. Most of the remaining lines are lightly loaded (below 15%) except L20, L21, and L22. From the perspective of line loading variation, all line loadings vary closely for Cases 2 and 3. Overall, Case 3a (%*LLI* = 217.094) exhibits the best line loading compared with other cases. Similar line loading characteristics can also be observed in Figure 9 (investigation category II). Case 5 and Case 6 have reduced line loading for almost all lines compared with Case 4. Cases with the same weighting factor (Case 5a and 6a) achieve lighter line loading than cases with more significance to *TOC* (Case 5b and Case 6b). Because cases with larger weight to *TOC* require bigger BESS capacity to compensate electricity shortage during the power outage, this might lead to more energy conversions and transmissions, causing heavier line loading and larger line losses. It is apparent that all system feeds in instigation categories I and II have adequate spare capacity to handle the worst scenario during an outage.

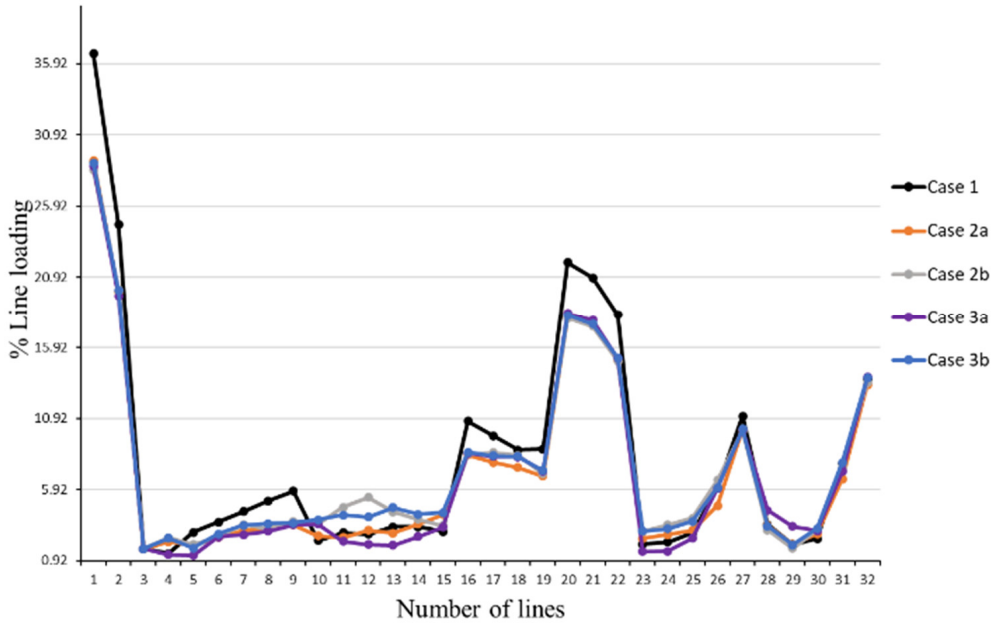

Figure 8. Line loading for investigation category I.

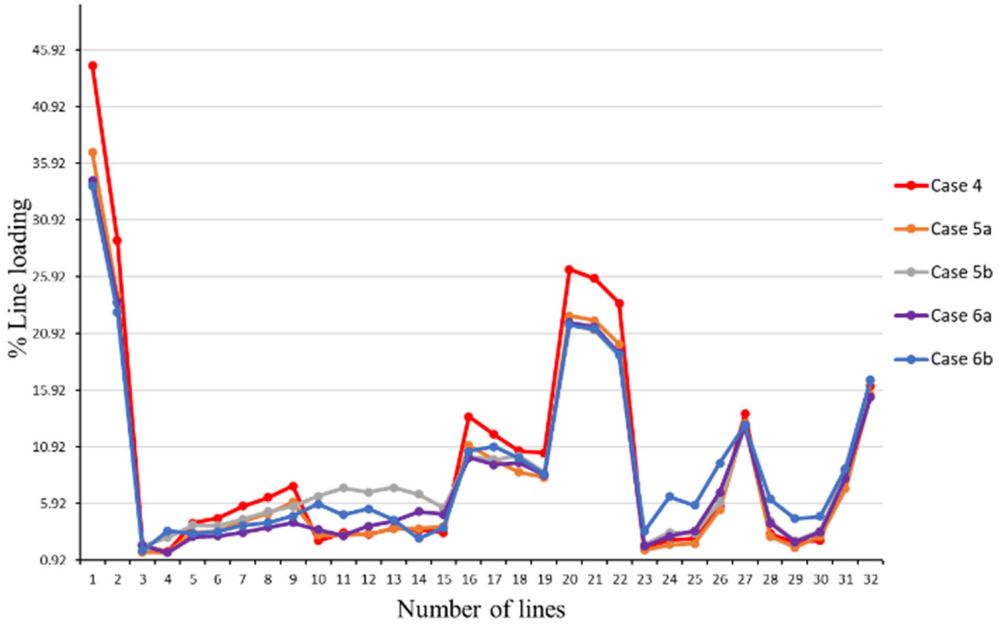

Figure 9. Line loading for investigation category II.

Figures 10 and 11 compare the total line losses for various cases. As referred to in Figure 10, L21 exhibits the highest line loss of around 0.032 MVA for Cases 2a and 3a and around 0.036 MVA for Cases 2b and 3b. Case 3b provides the worst line loss performance, especially at L10–L14, while a slightly higher line loss is noticed at L2, L26, and L32 for Case 2b. As illustrated in Figure 11, again, L21 exhibits the highest line loss of around 0.033 MVA for all cases with BESS allocation except for Case 6b, which has a slightly higher loss of about 0.037 MVA. Case 6b exhibits the largest total line loss, especially at L24-L26, while a slightly higher line loss is noticed at L10–L14 for Case 5b. On the whole, the total line loss in both investigation categories I and II has almost the same characteristics compared with each other. For investigation category I, the total line losses are slightly lower in Cases with the same weighting factor (Case 2a and 3a) than in cases with more significance to *TOC* (Case 2b and Case 3b). Similarly, Case 5a provides the minimum total line losses (0.163 MVA) for investigation category II, as illustrated in Figure 11.

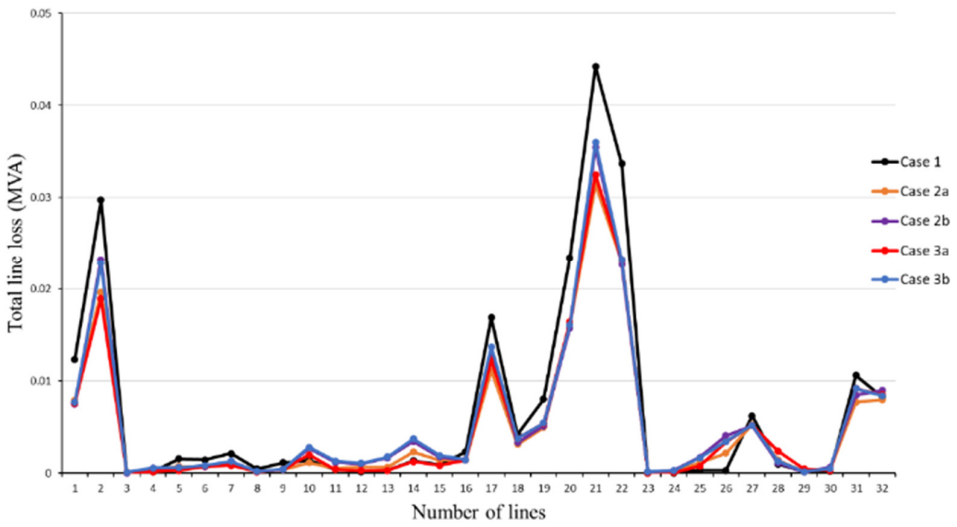

Figure 10. Total line loss for investigation category I.

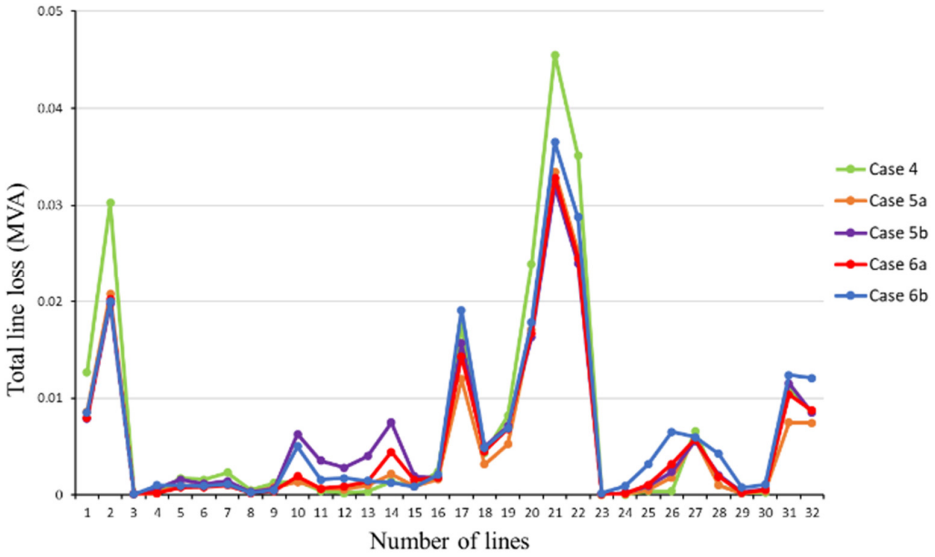

Figure 11. Total line loss for investigation category II.

6.4.4. Comparison of Optimization Results with Uniform Size and Non-Uniform Size BESS

To evaluate the difference between uniform and non-uniform BESS allocation techniques in terms of their impact on system performance and economic efficiency, a comparison between cases with uniform size BESS and cases with non-uniform size BESS is conducted for both categories I and II, as shown in Table 3. The comparison results show that most ratios are greater than 1, indicating that uniform BESS allocation is generally superior to non-uniform BESS allocation in terms of system performance and economic efficiency improvement in balanced and unbalanced systems.

Table 3. Comparison between cases with uniform size BESS and cases with non-uniform size BESS.

Cases Comparison	VDI Ratio	LLI Ratio	S_{TLoss} Ratio	TOC Ratio	Total BESS Size Ratio	Objective Function Value Ratio
Case 3a:2a	1.072	0.995	1.026	1.048	1.086	1.038
Case 3b:2b	0.995	1.006	1.017	1.027	0.986	1.015
Case 6a:5a	0.970	1.004	1.080	1.072	1.093	1.077
Case 6b:5b	1.172	0.999	1.077	1.035	1.048	1.058

6.4.5. Comparison of Optimization Results with EGWO, GWO, and PSO Algorithms

In this research, the widely used GWO approach [45–48] and PSO algorithm [49,50,71–75] are applied to evaluate the performance of the proposed EGWO approach for Case 2a, Case 3a, Case 5a, and Case 6a. The detailed formulation of the PSO technique is depicted in Appendix B. As recommended in [49,50,76], the inertia constant (α), the cognitive (b_1) and social coefficient (b_2) of PSO are set to 0.6, 1.8, and 1.8, respectively. Other parameters utilized during the PSO process are maximum iteration = 1000 and population size = 50, which are the same as the EGWO approach. The same GWO technique in [66] is also applied to validate the effectiveness of EGWO. The same settings (φ, γ, D, NF, Hmax) are utilized for both EGWO and GWO techniques, as shown in Table 1. Due to the stochastic nature of heuristic algorithms such as EGWO, GWO, and PSO approaches, all techniques are run 30 times to validate the optimality of the generated outcomes. Table 4 compares the best, worst, and mean results generated by EGWO, GWO, and PSO techniques. Moreover, the standard deviations (σ^{EGWO}, σ^{GWO}, and σ^{PSO}) of obtained solutions are also assessed. The greater σ denotes a larger variation in the outcomes of 30 optimization runs. Table 4 shows that the minimum objective function values are obtained from the EGWO technique, which are 776,708.934 USD/year and 801,762.079 USD/year for investigation categories I and II, respectively. In the meanwhile, the results of σ^{EGWO} are smaller than σ^{GWO} and σ^{PSO} in

both investigation categories. Therefore, the EGWO technique is superior compared with GWO and PSO in attaining the required optimal outcomes for both investigation categories according to the statistical analysis of Table 4.

Table 4. Statistical analysis of EGWO and PSO algorithm for 30 runs.

Optimization Statistics	Apparent Power per BESS (MVA) and Their Sites	VDI (%)	LLI (%)	S_{TLoss} (MVA)	TOC (USD/Year)	Total BESS Size (MWh)	Objective Function Value (USD/Year)
Investigation category I: uniform size BESS allocation							
EGWO best	BESS03, BESS06, BESS07, BESS08, BESS10, BESS11, BESS24, BESS27, BESS28, BESS30, BESS31, BESS32, BESS33, MVA for each BESS = 0.118	59.637	218.294	0.156	327,352	1.530	776,708.934
EGWO worst	BESS03, BESS06, BESS07, BESS08, BESS10, BESS11, BESS24, BESS27, BESS28, BESS30, BESS31, BESS32, BESS33, MVA for each BESS = 0.120	60.288	221.805	0.160	326,672	1.562	787,222.024
EGWO mean	BESS03, BESS06, BESS07, BESS08, BESS10, BESS11, BESS24, BESS27, BESS28, BESS30, BESS31, BESS32, BESS33, MVA for each BESS = 0.118	59.716	219.686	0.158	327,158	1.539	781,880.637
σ^{EGWO}							2254.229
GWO best	BESS03, BESS06, BESS07, BESS08, BESS10, BESS11, BESS24, BESS27, BESS28, BESS30, BESS31, BESS32, BESS33, MVA for each BESS = 0.118	59.717	219.135	0.156	328,066	1.534	777,584.154
GWO worst	BESS03, BESS06, BESS07, BESS08, BESS10, BESS11, BESS24, BESS27, BESS28, BESS30, BESS31, BESS32, BESS33, MVA for each BESS = 0.120	60.531	222.375	0.161	327,283	1.563	790,407.7772
GWO mean	BESS03, BESS06, BESS07, BESS08, BESS10, BESS11, BESS24, BESS27, BESS28, BESS30, BESS31, BESS32, BESS33, MVA for each BESS = 0.119	60.279	220.224	0.159	327,626	1.547	785,136.4344
σ^{GWO}							3168.572
PSO best	BESS03, BESS06, BESS07, BESS08, BESS10, BESS11, BESS24, BESS27, BESS28, BESS30, BESS31, BESS32, BESS33, MVA for each BESS = 0.119	59.827	220.335	0.157	329,390	1.541	781,691.030
PSO worst	BESS03, BESS06, BESS07, BESS08, BESS10, BESS11, BESS24, BESS27, BESS28, BESS30, BESS31, BESS32, BESS33, MVA for each BESS = 0.120	60.748	222.586	0.163	329,537	1.565	797,763.171
PSO mean	BESS03, BESS06, BESS07, BESS08, BESS10, BESS11, BESS24, BESS27, BESS28, BESS30, BESS31, BESS32, BESS33, MVA for each BESS = 0.120	61.427	220.659	0.160	329,366	1.557	789,727.676
σ^{PSO}							3801.475
Investigation category I: non-uniform size BESS allocation							
EGWO best	BESS03 = 0.154, BESS06 = 0.140, BESS07 = 0.212, BESS10 = 0.101, BESS12 = 0.221, BESS15 = 0.123, BESS16 = 0.141, BESS20 = 0.102, BESS21 = 0.228, BESS32 = 0.117, BESS33 = 0.123	63.918	217.094	0.160	343,117	1.662	806,494.357

Table 4. *Cont.*

Optimization Statistics	Apparent Power per BESS (MVA) and Their Sites	VDI (%)	LLI (%)	S_{TLoss} (MVA)	TOC (USD/Year)	Total BESS Size (MWh)	Objective Function Value (USD/Year)
EGWO worst	BESS03 = 0.170, BESS06 = 0.144, BESS07 = 0.201, BESS10 = 0.111, BESS12 = 0.227, BESS15 = 0.132, BESS16 = 0.144, BESS20 = 0.117, BESS21 = 0.202, BESS32 = 0.122, BESS33 = 0.124	64.534	218.904	0.164	342,514	1.694	817,002.887
EGWO mean	BESS03 = 0.165, BESS06 = 0.147, BESS07 = 0.207, BESS10 = 0.106, BESS12 = 0.217, BESS15 = 0.133, BESS16 = 0.143, BESS20 = 0.109, BESS21 = 0.214, BESS32 = 0.108, BESS33 = 0.113	64.441	217.825	0.164	343,248	1.664	816,784.140
σ^{EGWO}							2803.794
GWO best	BESS03 = 0.179, BESS06 = 0.14, BESS07 = 0.173, BESS10 = 0.105, BESS12 = 0.222, BESS15 = 0.126, BESS16 = 0.131, BESS20 = 0.109, BESS21 = 0.222, BESS32 = 0.134, BESS33 = 0.122	64.204	217.155	0.16	343,325	1.664	806,769.3473
GWO worst	BESS03 = 0.164, BESS06 = 0.143, BESS07 = 0.209, BESS10 = 0.127, BESS12 = 0.243, BESS15 = 0.112, BESS16 = 0.142, BESS20 = 0.108, BESS21 = 0.224, BESS32 = 0.129, BESS33 = 0.128	65.062	219.344	0.165	342,104	1.727	820,125.514
GWO mean	BESS03 = 0.173, BESS06 = 0.135, BESS07 = 0.221, BESS10 = 0.12, BESS12 = 0.22, BESS15 = 0.134, BESS16 = 0.136, BESS20 = 0.103, BESS21 = 0.228, BESS32 = 0.114, BESS33 = 0.106	65.166	218.193	0.164	342,756	1.69	817,100.0288
σ^{GWO}							3472.036
PSO best	BESS03 = 0.160, BESS06 = 0.138, BESS07 = 0.223, BESS10 = 0.109, BESS12 = 0.225, BESS15 = 0.127, BESS16 = 0.136, BESS20 = 0.1, BESS21 = 0.213, BESS32 = 0.1, BESS33 = 0.134	64.666	217.269	0.160	343,460	1.665	806,946.377
PSO worst	BESS03 = 0.166, BESS06 = 0.144, BESS07 = 0.219, BESS10 = 0.149, BESS12 = 0.256, BESS15 = 0.112, BESS16 = 0.151, BESS20 = 0.102, BESS21 = 0.237, BESS32 = 0.108, BESS33 = 0.122	66.225	219.982	0.168	341,361	1.769	828,231.884
PSO mean	BESS03 = 0.158, BESS06 = 0.138, BESS07 = 0.223, BESS10 = 0.130, BESS12 = 0.225, BESS15 = 0.127, BESS16 = 0.156, BESS20 = 0.1, BESS21 = 0.233, BESS32 = 0.1, BESS33 = 0.127	66.179	218.974	0.165	342,384	1.719	820,163.831
σ^{PSO}							4903.673
	Investigation category II: uniform size BESS allocation						
EGWO best	BESS05, BESS06, BESS07, BESS08, BESS09, BESS18, BESS24, BESS25, BESS26, BESS29, BESS30, BESS31, BESS32, BESS33, MVA for each BESS = 0.112	69.589	265.765	0.163	331,112	1.573	801,762.079
EGWO worst	BESS05, BESS06, BESS07, BESS08, BESS09, BESS18, BESS24, BESS25, BESS26, BESS29, BESS30, BESS31, BESS32, BESS33, MVA for each BESS = 0.115	70.355	270.044	0.170	330,417	1.607	819,900.770

Table 4. *Cont.*

Optimization Statistics	Apparent Power per BESS (MVA) and Their Sites	VDI (%)	LLI (%)	S_{TLoss} (MVA)	TOC (USD/Year)	Total BESS Size (MWh)	Objective Function Value (USD/Year)
EGWO mean	BESS05, BESS06, BESS07, BESS08, BESS09, BESS18, BESS24, BESS25, BESS26, BESS29, BESS30, BESS31, BESS32, BESS33, MVA for each BESS = 0.114	69.680	267.466	0.168	330,649	1.594	814,582.039
σ^{EGWO}							3681.945
GWO best	BESS05, BESS06, BESS07, BESS08, BESS09, BESS18, BESS24, BESS25, BESS26, BESS29, BESS30, BESS31, BESS32, BESS33, MVA for each BESS = 0.113	69.803	266.211	0.164	333,676	1.581	807,104.5086
GWO worst	BESS05, BESS06, BESS07, BESS08, BESS09, BESS18, BESS24, BESS25, BESS26, BESS29, BESS30, BESS31, BESS32, BESS33, MVA for each BESS = 0.117	70.61	269.904	0.171	332,230	1.631	824,944.8592
GWO mean	BESS05, BESS06, BESS07, BESS08, BESS09, BESS18, BESS24, BESS25, BESS26, BESS29, BESS30, BESS31, BESS32, BESS33, MVA for each BESS = 0.114	70.193	267.448	0.169	332,870	1.602	819,563.6258
σ^{GWO}							4782.519
PSO best	BESS05, BESS06, BESS07, BESS08, BESS09, BESS18, BESS24, BESS25, BESS26, BESS29, BESS30, BESS31, BESS32, BESS33, MVA for each BESS = 0.113	69.965	267.053	0.165	336,410	1.588	812,605.067
PSO worst	BESS05, BESS06, BESS07, BESS08, BESS09, BESS18, BESS24, BESS25, BESS26, BESS29, BESS30, BESS31, BESS32, BESS33, MVA for each BESS = 0.119	71.035	269.777	0.173	336,545	1.660	835,158.116
PSO mean	BESS05, BESS06, BESS07, BESS08, BESS09, BESS18, BESS24, BESS25, BESS26, BESS29, BESS30, BESS31, BESS32, BESS33, MVA for each BESS = 0.115	70.917	267.427	0.171	336,383	1.611	828,384.203
σ^{PSO}							5216.346
	Investigation category II: non-uniform size BESS allocation						
EGWO best	BESS02 = 0.127, BESS03 = 0.161, BESS06 = 0.232, BESS08 = 0.131, BESS10 = 0.159, BESS11 = 0.140, BESS17 = 0.158, BESS28 = 0.232, BESS29 = 0.108, BESS32 = 0.115, BESS33 = 0.157	67.519	266.914	0.176	355,030	1.720	862,798.837
EGWO worst	BESS02 = 0.151, BESS03 = 0.154, BESS06 = 0.212, BESS08 = 0.132, BESS10 = 0.157, BESS11 = 0.152, BESS17 = 0.155, BESS28 = 0.248, BESS29 = 0.109, BESS32 = 0.111, BESS33 = 0.162	68.167	269.130	0.183	354,391	1.743	880,563.532
EGWO mean	BESS02 = 0.142, BESS03 = 0.159, BESS06 = 0.231, BESS08 = 0.133, BESS10 = 0.159, BESS11 = 0.156, BESS17 = 0.155, BESS28 = 0.230, BESS29 = 0.1, BESS32 = 0.1, BESS33 = 0.158	68.072	267.795	0.182	355,172	1.721	878,105.437
σ^{EGWO}							4087.372
GWO best	BESS02 = 0.184, BESS03 = 0.189, BESS06 = 0.211, BESS08 = 0.144, BESS10 = 0.161, BESS11 = 0.126, BESS17 = 0.159, BESS28 = 0.245, BESS29 = 0.115, BESS32 = 0.115, BESS33 = 0.1	67.932	266.971	0.175	356,921	1.749	863,054.3303

Table 4. *Cont.*

Optimization Statistics	Apparent Power per BESS (MVA) and Their Sites	VDI (%)	LLI (%)	S_{TLoss} (MVA)	TOC (USD/Year)	Total BESS Size (MWh)	Objective Function Value (USD/Year)
GWO worst	BESS02 = 0.15, BESS03 = 0.149, BESS06 = 0.198, BESS08 = 0.151, BESS10 = 0.145, BESS11 = 0.145, BESS17 = 0.168, BESS28 = 0.26, BESS29 = 0.108, BESS32 = 0.107, BESS33 = 0.201	68.859	269.61	0.185	355,641	1.784	888,104.5267
GWO mean	BESS02 = 0.135, BESS03 = 0.164, BESS06 = 0.223, BESS08 = 0.15, BESS10 = 0.149, BESS11 = 0.146, BESS17 = 0.149, BESS28 = 0.24, BESS29 = 0.099, BESS32 = 0.109, BESS33 = 0.184	68.212	268.275	0.183	355,560	1.752	881,962.4297
σ^{GWO}							5653.736
PSO best	BESS02 = 0.153, BESS03 = 0.179, BESS06 = 0.231, BESS08 = 0.153, BESS10 = 0.168, BESS11 = 0.131, BESS17 = 0.164, BESS28 = 0.242, BESS29 = 0.1, BESS32 = 0.1, BESS33 = 0.102	68.153	267.013	0.175	357,870	1.723	863,228.487
PSO worst	BESS02 = 0.162, BESS03 = 0.165, BESS06 = 0.202, BESS08 = 0.164, BESS10 = 0.151, BESS11 = 0.148, BESS17 = 0.177, BESS28 = 0.259, BESS29 = 0.114, BESS32 = 0.101, BESS33 = 0.192	69.795	270.351	0.187	357,798	1.837	896,928.444
PSO mean	BESS02 = 0.156, BESS03 = 0.182, BESS06 = 0.230, BESS08 = 0.157, BESS10 = 0.151, BESS11 = 0.144, BESS17 = 0.160, BESS28 = 0.238, BESS29 = 0.107, BESS32 = 0.1, BESS33 = 0.203	70.143	269.096	0.182	356,188	1.829	882,453.006
σ^{PSO}							7252.429

Figures 12 and 13 present the convergence characteristics of EGWO, GWO, and PSO techniques for investigation categories I and II, respectively. Table 5 illustrates the convergence and computation time of EGWO, GWO, and PSO techniques in all cases. Table 5 and Figures 12 and 13 suggest that EGWO, GWO, and PSO approaches take more iteration and computation time to converge in the unbalanced system (investigation category II) than the balanced system (investigation category I). For example, the EGWO approach for uniform BESS allocation converges after 239 iterations (581 s) and 256 iterations (611 s) in balanced and unbalanced systems, respectively. Accordingly, the GWO approach takes 262 iterations (642 s) and 285 iterations (681 s) to reach convergence in balanced and unbalanced systems, respectively. On the other hand, the PSO approach takes 293 iterations (716 s) and 311 iterations (742 s) to reach convergence in balanced and unbalanced systems, respectively. Moreover, uniform BESS allocation converges faster than non-uniform BESS allocation. Moreover, in all cases, the EGWO approach requires fewer iterations and computation time to reach convergency than GWO and PSO algorithms.

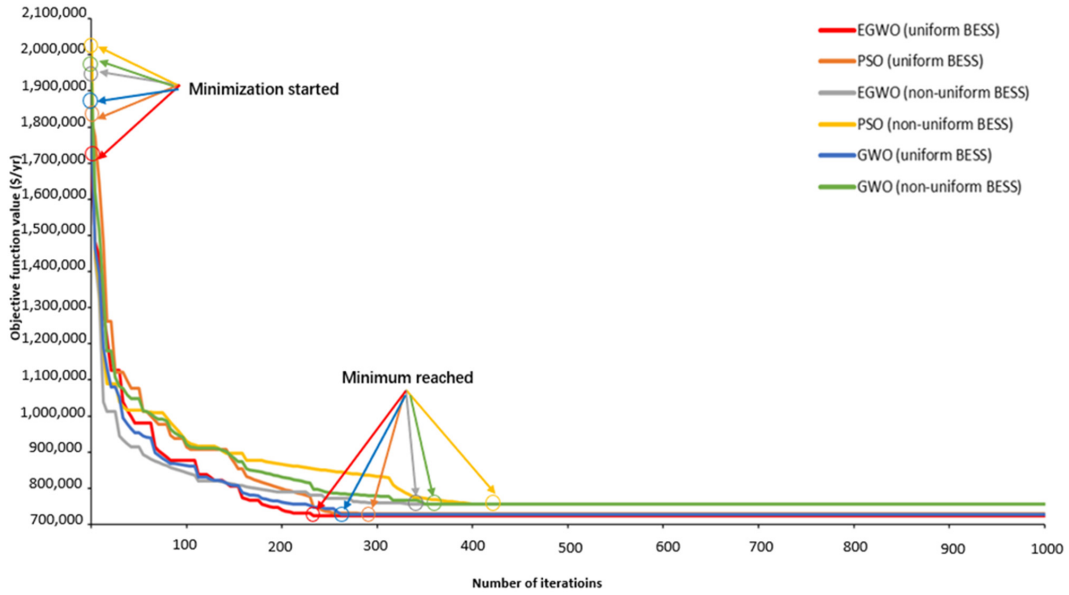

Figure 12. Convergence of EGWO, GWO, and PSO approaches for investigation category I.

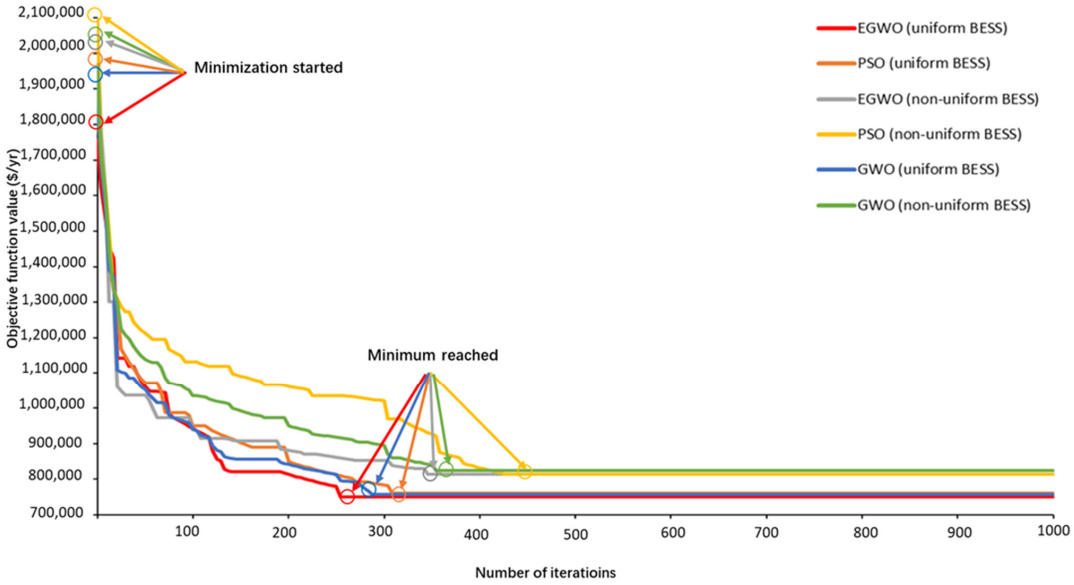

Figure 13. Convergence of EGWO, GWO, and PSO approaches for investigation category II.

Table 5. Convergence and computation time of EGWO, GWO, and PSO approaches.

Investigation Category	BESS Allocation	EGWO Convergence	EGWO Computation Time (s)	GWO Convergence	GWO Computation Time (s)	PSO Convergence	PSO Computation Time (s)
I	Uniform BESS	After 239 iterations	581	262	642	After 293 iterations	716
	Non-uniform BESS	After 340 iterations	774	357	799	After 428 iterations	945
II	Uniform BESS	After 256 iterations	611	285	681	After 311 iterations	742
	Non-uniform BESS	After 346 iterations	810	367	821	After 440 iterations	983

6.5. Reliability and BESS Cost

Improvement of reliability performance for both investigation categories compared with their base case is tabulated in Table 6. The results indicate the integration of BESS

caused a significant impact on system reliability. The improvement of reliability parameters for all cases in balanced and unbalanced systems are calculated based on their base cases, as shown in Table 6. It is noticeable that all reliability parameters significantly improved compared with their base cases. Cases with larger weighting factor (Case 2b, 3b, 5b, and 6b) of the system reliability have greater improvement, usually above 25%, of cases with the same weighting factor (Case 2a, 3a, 5a, and 6a).

Table 6. Reliability improvement for both investigation categories compared with their base case.

	Improved Cost Saving of EIC (%)	Improved Cost Saving of Cost of EENS (%)	Improved Cost Saving of TOC (%)	Reduced SAIDI (%)
Case 1	–	–	–	–
Case 2a	20.010	19.536	19.739	14.522
Case 2b	26.314	25.997	26.193	23.781
Case 3a	15.694	15.923	15.874	11.806
Case 3b	23.981	24.240	24.194	29.138
Case 4	–	–	–	–
Case 5a	25.742	25.577	25.673	24.770
Case 5b	30.577	30.547	30.659	30.245
Case 6a	19.838	20.480	20.304	20.634
Case 6b	28.252	27.933	28.238	34.185

Figure 14 compares reliability performance and total BESS capacity. It is noticeable that all the reliability parameters have a larger improvement in the unbalanced system compared with the balanced system while demanding more BESS installation. In terms of TOC improvement, which is the main focus regarding system reliability in this research, Case 2a is relatively cost efficient than other cases in investigation category I, representing the optimal choice for BESS allocation in balanced distribution systems. Similarly, Case 5a represents the optimal choice for BESS allocation in unbalanced distribution systems.

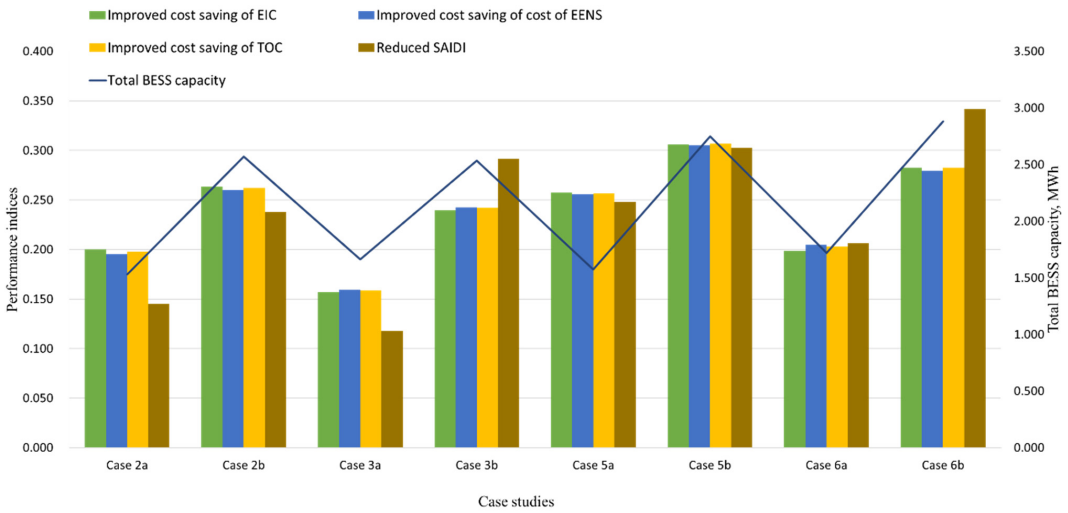

Figure 14. Reliability performance and BESS capacity comparison for all cases.

6.6. Overall Performance and BESS Cost Comparison

The performance parameters for balanced and unbalanced systems are calculated and tabulated in Tables 7 and 8, respectively. Usually, VPII greater than one denotes a good voltage profile. The bigger the VPII value, the better the voltage profile. For example, VPII = 2.35 for Case 2b indicates that Case 2b achieves the best voltage profile in balanced distribution systems for all cases. Contrary to VPII, the higher value of $PLsRI^{P}$, $PLsRI^{Q}$, $PLsRI^{T}$, LLI, and TOCRI represent the worse real power loss, reactive power loss, total line loss, line loading, and system reliability, respectively. For instance, $PLsRI^{T}$ = 0.748 and TOCRI = 0.841 in Case 3a are larger than the results in Case 2a, representing that line loss and system reliability in Case 3a are worse than in Case 2a. VPII and LLI have the smaller value in Case

3a compared with Case 2a, indicating Case 3a has a worse voltage profile and better line loading than Case 2a. According to Tables 7 and 8, VPII, $PLsRI^P$, $PLsRI^Q$, $PLsRI^T$, and LLI in investigation category II are generally higher than in investigation category I, which indicates that the voltage profile has a larger improvement in the unbalanced system compared with the balanced system. However, the improvement in real power loss, reactive power loss, total line loss, and line loading in the unbalanced system is smaller than in the balanced system due to the increased deployment of BESS. Because unbalanced distribution networks are more complex and require more energy storage systems to meet the system's needs. This might lead to more energy conversions and transmissions, resulting in less reduction in real power loss, reactive power loss, total line loss, and line loading compared with the balanced systems. In practice, if a greater improvement in these performance parameters is needed, the corresponding weighting factor in Equation (9) can be increased during optimization. Additionally, TOCRI in investigation category II is usually smaller than in investigation category I, representing that reliability has a larger improvement in the unbalanced system compared with the balanced system.

Table 7. Performance improvement of all cases in investigation category I.

Case Studies	VPII	$PLsRI^P$	$PLsRI^Q$	$PLsRI^T$	LLI	TOCRI
Case 1	–	–	–	–	–	–
Case 2a	1.609	0.716	0.748	0.729	0.852	0.803
Case 2b	2.350	0.796	0.838	0.813	0.903	0.738
Case 3a	1.501	0.729	0.775	0.748	0.847	0.841
Case 3b	2.361	0.806	0.855	0.827	0.908	0.758

Table 8. Performance improvement of all cases in investigation category II.

Case Studies	VPII	$PLsRI^P$	$PLsRI^Q$	$PLsRI^T$	LLI	TOCRI
Case 4	–	–	–	–	–	–
Case 5a	1.385	0.740	0.742	0.741	0.859	0.743
Case 5b	4.135	0.875	0.917	0.882	0.943	0.693
Case 6a	1.428	0.790	0.842	0.800	0.863	0.797
Case 6b	3.528	0.938	0.997	0.950	0.941	0.718

Figure 15 compares overall system performance and total BESS capacity. It is noticeable that Case 2a is relatively cost efficient than other cases in investigation category I, representing the optimal choice for BESS allocation in balanced distribution systems. Similarly, Case 5a represents the optimal choice for BESS allocation in unbalanced distribution systems.

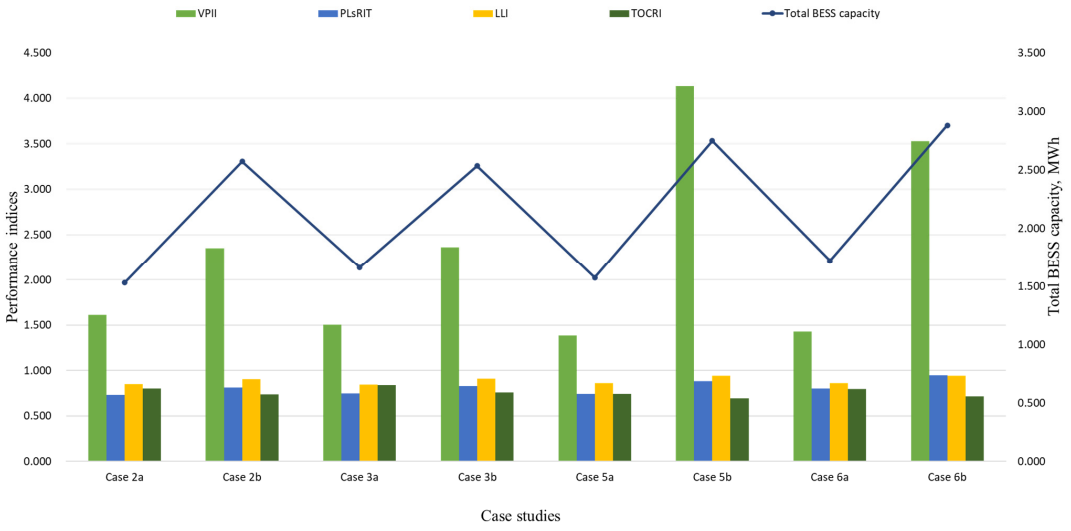

Figure 15. Performance and BESS capacity comparison for all cases.

7. Conclusions

This paper proposes an effective methodology using the EGWO algorithm to optimally allocate BESS into distribution networks to enhance system reliability, improve power quality, and reduce power losses, line loading, and investment cost for BESS. The efficacy of the proposed methodology has been demonstrated in an IEEE 33 bus distribution network. The system performance improvement is evaluated through relevant performance indices. The solutions generated from the EGWO approach are verified by the GWO and PSO approach. Utilities may use the results of this study as a benchmark to improve the reliability and efficiency of distribution systems. The conclusions according to the simulation outcomes of the proposed BESS allocation method are summarized below:

- A considerable reduction in TOC (19.739% and 25.673% reduction in balanced and unbalanced systems, respectively) of the wind and solar DGs penetrated distribution system is achieved with the application of BESSs, thereby improving system reliability.
- Both BESS allocation methodologies with uniform and non-uniform BESS sizes can be used to improve the system performance and economic efficiency in both balanced and unbalanced distribution systems. Nevertheless, BESS allocation with non-uniform BESS size is more regulatable in terms of system performance and economic efficiency improvement.
- The unbalanced distribution systems demand more BESS installation compared with the balanced system, leading to a larger improvement in system reliability and voltage profile; however, it also aggravates the line loading and power loss in the unbalanced system.
- A significant reduction in required iteration (18.892% on average compared with PSO, 7.905% on average compared with GWO) and computation time (18.202% on average compared with PSO, 7.637% on average compared with GWO) to reach convergency in all cases is achieved by the proposed EGWO technique. Furthermore, EGWO, GWO, and PSO approaches take more iteration (4.439% on average for EGWO, 5.79% on average for GWO, 4.474% on average for PSO) and computation time (4.907% on average for EGWO, 4.414% in average for GWO, 3.826% in average for PSO) to converge in the unbalanced system than the balanced system. Moreover, uniform BESS allocation converges faster than non-uniform BESS allocation.

Regarding future work, optimal BESS operation incorporating smart charging and discharging techniques can be investigated for further improving the system performance. The BESS model can also take memory effect and self-discharge into account. Furthermore, new optimal BESS allocation strategies can be proposed by jointly planning with other solutions and devices, such as electric vehicle charging stations, renewable DGs, synchronous condensers, or DFACTS, for achieving better system performance and economic efficiency.

Author Contributions: Conceptualization, D.Z., G.S., C.K.D. and K.W.W.; methodology, D.Z., G.S., C.K.D. and K.W.W.; software, D.Z., G.S. and C.K.D.; validation, D.Z., G.S. and C.K.D. and K.W.W.; formal analysis, D.Z., G.S., C.K.D. and K.W.W.; investigation, D.Z., G.S., C.K.D. and K.W.W.; resources, G.S. and C.K.D.; data curation, D.Z. and C.K.D.; writing—original draft preparation, D.Z.; writing—review and editing, G.S., C.K.D. and K.W.W.; visualization, G.S., C.K.D. and K.W.W.; supervision, G.S. and C.K.D.; project administration, G.S. and C.K.D.; funding acquisition, D.Z. and G.S. All authors have read and agreed to the published version of the manuscript.

Funding: This research received no external funding.

Institutional Review Board Statement: Not applicable.

Informed Consent Statement: Not applicable.

Data Availability Statement: Not applicable.

Acknowledgments: The first author received support from Murdoch University (MU) International Tuition Fee Scholarship (ITFS) for PhD study. This research was developed as part the PhD research and hence, would like to acknowledge MU for their assistance.

Conflicts of Interest: The authors declare no conflict of interest.

Nomenclature

Δt	time interval (h)
η_c	BESS charging efficiency
η_d	BESS discharging efficiency
Obj	objective function (USD)
E_{max}	maximum BESS energy (kWh)
E_{min}	minimum BESS energy (kWh)
E_{ESS}	BESS energy (kWh)
E_{t+1}	BESS energy at time t + 1 (kWh)
E_t	BESS energy at time t (kWh)
H	iteration number
e	exponential value for power computation
K	total number of BESSs in service
L	total number of lines
B	total number of buses
$M_{m,site}$	BESS site info at bus m
$M_{m,size}$	BESS size info at bus m
P_{max}	maximum BESS power (MW)
P_{min}	minimum BESS power (MW)
P_{ESS}	BESS power (MW)
P_{md}^{del}	real power delivered from bus m to bus d (MW)
P_m^{con}	real power consumed at bus m (MW)
P_m^{gen}	real power generated at bus m (MW)
$P_{nm,}^{del}$	power delivered from bus n to bus m (MW)
P_{TLoss}	total real power loss (MW)
$P_{Loss}(m,n)$	real power loss of the line connecting bus m and n (MW)
P_c^t	BESS charging power at time t (MW)
P_d^t	BESS discharging power at time t (MW)
P_{ESS}^t	BESS power at time t (MW)
P^{TF}	input real power of the feeder (MW)
Q_{md}^{del}	reactive power delivered from bus m to bus d (MVar)
Q_m^{con}	reactive power consumed at bus m (MVar)
Q_m^{gen}	reactive power generated at bus m (MVar)
Q_{nm}^{del}	reactive power delivered from bus n to bus m (MVar)
$Q_{Loss}(m,n)$	reactive power loss of the line connecting two buses m and n (MVar)
Q^{TF}	input reactive power of the feeder (MVar)
$R(m,n)$	resistance of the line connecting buses m and n
$M_{size,max}$	maximum BESS size (MWh)
$M_{size,min}$	minimum BESS size (MWh)
M_{Lm}	load at bus m (p.u.)
NF	number of food sources
L_{ESS}^l	loading of line l after BESS placement (p.u.)
L_{rated}^l	rated ampacity of line l (p.u.)
S_{ESS}^k	state of charge of kth BESS
S^{Wind}	total capacity of wind DGs
S^{PV-Max}	maximum PV capacity
S^{PV-OP}	operational capacity of PV
$S^{BESS-Max}$	Maximum BESS capacity
C_U	cost rate of battery unit (USD/MWh/yr)
ub	upper boundary
lb	lower boundary
V_{bm}	voltage at bus m
V_{bm}^t	bus voltage at time t
V_{max}	maximum voltage limit (p.u.)
V_{min}	minimum voltage limit (p.u.)
V_{target}	system target voltage
V^{Rated}	system rated voltage (p.u.)
$X(m,n)$	reactance of a line connecting buses m and n
$LPEIC_{m,x}$	average interruption cost for load point m and contingency case x
IEEE-RTS	IEEE reliability test system

Appendix A. Feeder and Load Data for the Balanced and Unbalanced IEEE33-Bus Test System

Table A1. Feeder and load data for the balanced IEEE 33-bus test system [67].

Line Number	Sending Bus	Receiving Bus	Resistance (Ω)	Reactance (Ω)	Load at Receiving Bus	
					Real Power (kW)	Reactive Power (kVAr)
1	1	2	0.0922	0.0417	100	60
2	2	3	0.493	0.2511	90	40
3	3	4	0.366	0.1864	120	80
4	5	6	0.819	0.707	60	20
5	7	8	1.7114	1.2351	200	100
6	8	9	1.03	0.74	60	20
7	9	10	1.04	0.74	60	20
8	10	11	0.1966	0.065	45	30
9	11	12	0.3744	0.1238	60	35
10	12	13	14.68	1.155	60	35
11	13	14	0.5416	0.7129	120	80
12	14	15	0.591	0.526	60	10

Table A1. *Cont.*

Line Number	Sending Bus	Receiving Bus	Resistance (Ω)	Reactance (Ω)	Load at Receiving Bus	
					Real Power (kW)	Reactive Power (kVAr)
13	15	16	0.7463	0.545	60	20
14	16	17	1.289	1.721	60	20
15	17	18	0.732	0.574	90	40
16	2	19	0.164	0.1565	90	40
17	19	20	1.5042	1.3154	90	40
18	20	21	0.4095	0.4784	90	40
19	21	22	0.7089	0.9373	90	40
20	3	23	0.4512	0.3083	90	50
21	23	24	0.898	0.7091	420	200
22	24	25	0.896	0.7011	420	200
23	6	26	0.203	0.1034	60	25
24	26	27	0.2842	0.1447	60	25
25	27	28	1.059	0.9337	60	20
26	28	29	0.8042	0.7006	120	70
27	29	30	0.5075	0.2585	200	600
28	30	31	0.9744	0.963	150	70
29	31	32	0.3105	0.3619	210	100
30	32	33	0.341	0.5302	60	40
31 *	12	22	0	2	90	40
32 *	25	29	0	0.5	120	70

* Tie Lines, Substation Voltage =12.66 kV.

Table A2. Unbalanced load data for the IEEE 33-bus test system [68].

Bus#	Phase A		Phase B		Phase C	
	P Load (kW)	Q Load (kVAr)	P Load (kW)	Q Load (kVAr)	P Load (kW)	Q Load (kVAr)
1	0	0	0	0	0	0
2	45.38364	27.20091	46.97678	28.15615	7.651557	4.586019
3	40.39426	17.96903	41.40079	18.41674	8.280372	3.683133
4	49.86655	33.22193	24.70916	16.46191	45.47072	30.29369
5	20.16107	10.0808	13.36378	6.68189	26.41769	13.20885
6	26.5972	8.889419	28.53333	9.536398	4.813076	1.608633
7	44.63782	22.31891	92.25998	46.12999	63.12615	31.56307
8	59.19779	29.59916	58.84519	29.42233	81.98097	40.99049
9	15.41424	5.151792	27.3318	9.135175	17.19704	5.747483
10	24.80639	8.291057	18.93923	6.329818	16.19692	5.413576
11	18.15976	12.08478	21.68315	14.42961	5.194532	3.457145
12	13.46956	7.851367	14.87785	8.671978	31.59566	18.41674
13	22.79707	13.28792	26.14736	15.24114	10.99865	6.411024
14	54.15552	36.07964	35.9386	23.94304	29.95177	19.95485
15	12.29795	2.038706	11.59487	1.922239	36.05026	5.976143
16	17.19276	5.746415	26.55286	8.87446	16.19692	5.413576
17	14.27842	4.772473	25.79636	8.621759	19.8683	6.640218
18	34.66922	15.42225	15.7973	7.027551	39.60784	17.6191
19	38.60558	17.173	42.71238	19.00014	8.756925	3.895766
20	29.79417	13.25372	40.05341	17.8173	20.22732	8.997872
21	18.95633	8.432634	37.82504	16.82627	33.29352	14.81053
22	42.80748	19.04234	40.01441	17.80021	7.252471	3.226348
23	22.80081	12.65803	21.40855	11.88497	45.86553	25.46245
24	143.0973	68.16254	125.6069	59.83088	151.2179	72.03053
25	137.0501	65.28186	209.1078	99.60541	73.76417	35.13669
26	22.06835	9.205162	28.87098	12.04257	9.003749	3.755792
27	19.7903	8.254728	18.74103	7.817175	21.41175	8.931091
28	25.42879	8.498881	24.85768	8.308153	9.656605	3.227416
29	37.73101	22.01385	22.12872	12.91073	60.18723	35.11585
30	39.19273	117.5782	86.54295	259.6283	74.28828	222.8654
31	57.7863	26.97919	26.62017	12.4283	65.61202	30.63294
32	73.98108	35.2398	85.37026	40.66513	50.60969	24.10705
33	12.19644	8.152686	14.31956	9.571659	33.42708	22.34456

Appendix B. PSO Technique

The flowchart of the PSO approach is depicted in Figure A1. The PSO is a bio-inspired metaheuristic technique proposed by Everhart and Kennedy in 1995 [77]. This algorithm simulated the movement of an insect swarm or bird flock to find the global optimum of the problem. The whole population follows the individual who knows the optimum position, such as a food source [78]. Furthermore, individuals also move based on their instinct. Each individual is considered a particle. The position of particle i, x_i, represents a possible solution of the problem that has the fitness $f(x_i)$.

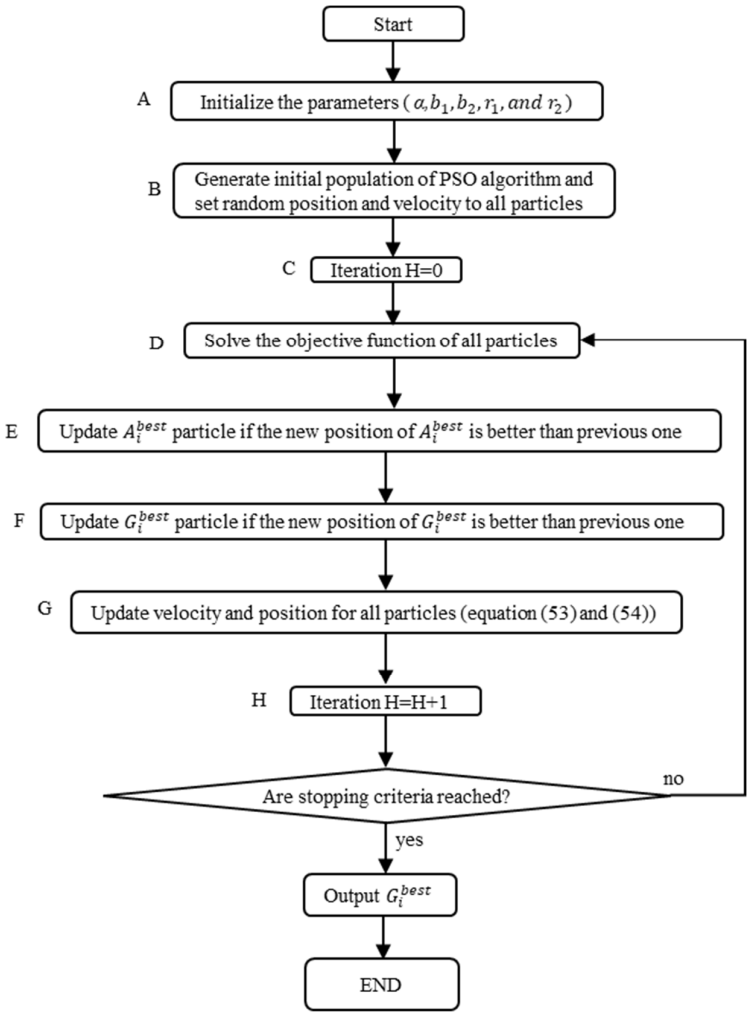

Figure A1. Flowchart of PSO approach.

In each iteration of PSO, as shown in (A1), A_i^{best} and G_i^{best} must be updated. Particle-best, A_i^{best}, represents the best fitness point that particle i has searched. Global-best, G_i^{best}, represents the best fitness point that the whole population has visited up to iteration H:

$$G_i^{best}(H) = argmax_{A_i^{best}} f\left(A_i^{best}(H)\right) \quad \text{(A1)}$$

Three factors that determine the particle's movement are the particle's inertia, particle best, and global best. Firstly, the inertia of the particles maintains them on the present trajectory. Secondly, particles also move towards the particle best, A_i^{best}. Thirdly, particles are also attracted by the global best, G_i^{best}. The mathematical expression of particle i's velocity v_i and position x_i are illustrated in (A2) and (A3), respectively [78].

$$v_i(H+1) = \alpha v_i(H) + b_1 r_1(H+1)\left[A_i^{best}(H) - x_i(H)\right] + b_2 r_2(H+1)\left[G_i^{best}(H) - x_i(H)\right] \quad \text{(A2)}$$

$$x_i(H+1) = x_i(H) + x_i(H+1) \quad \text{(A3)}$$

where V_i represents the velocity of ith particle. α is the inertia constant, which is usually less than 1. r_1 and r_2 are random numbers selected from interval [0, 1]. $v_i(H)$ and $x_i(H)$ are the velocity and position of ith particle at Hth iteration, respectively in which H is the iteration number. Cognitive coefficient, b_1, represents the particle's own instinct about the optimum. Social coefficient, b_2, integrates the behavior of the whole population. The value of the above PSO parameters utilized in this research is presented in Table A3.

Table A3. PSO parameters and variables.

Type	Parameters/Variables	Description/Settings
Input parameters	$V^{Rated}, R(m,n), X(m,n), P, Q, P^{TF}, Q^{TF}, S^{Wind}, S^{PV-Max}, S^{PV-OP}$, and $S^{BESS-Max}$	Critical for the distribution system model
Output parameters	TOC, VDC, PLC, LLC, and BESSC	Critical for the objective function
Decision variables	$M_{m,size}$	Determine the sizes of BESSs in MVA with a unity power factor.
	$M_{m,site}$	Determine the locations of BESSs in the grid.
PSO parameters	$\alpha, b_1, b_2, SS, J_{trail}, H_{max}$	Settings: α = inertia constant = 0.6, b_1 = cognitive coefficient = b_2 = social coefficient = 1.8, SS = swarm size = 100, J_{trail} = trail limit to improve a food source = 60, H_{max} = maximum iteration = 1000
PSO bounds	For $M_{m,site}$: lb1, and ub1 For $M_{m,size}$: lb2, and ub2	Settings: lb1 = 0.1 MVA and ub1 = 2 MVA Settings: lb2 = 0 and ub2 = 1

References

1. Zhang, D.; Shafiullah, G.; Das, C.K.; Wong, K.W. A systematic review of optimal planning and deployment of distributed generation and energy storage systems in power networks. *J. Energy Storage* **2022**, *56*, 105937. [CrossRef]
2. Shafiullah, G. Hybrid renewable energy integration (HREI) system for subtropical climate in Central Queensland, Australia. *Renew. Energy* **2016**, *96*, 1034–1053. [CrossRef]
3. Goel, L. Power system reliability cost/benefit assessment and application in perspective. *Comput. Electr. Eng.* **1998**, *24*, 315–324. [CrossRef]
4. International Energy Agency. Renewable Electricity Growth is Accelerating Faster than Ever Worldwide, Supporting the Emergence of the New Global Energy Economy. 1 December 2021. Available online: https://www.iea.org/news/renewable-electricity-growth-is-accelerating-faster-than-ever-worldwide-supporting-the-emergence-of-the-new-global-energy-economy (accessed on 13 May 2023).
5. Billinton, R.; Allan, R.N. *Reliability Evaluation of Engineering Systems*; Springer: Berlin/Heidelberg, Germany, 1992; Volume 792.
6. Li, W. *Reliability Assessment of Electric Power Systems Using Monte Carlo Methods*; Springer Science & Business Media: Berlin/Heidelberg, Germany, 2013.
7. Adefarati, T.; Bansal, R. Reliability and economic assessment of a microgrid power system with the integration of renewable energy resources. *Appl. Energy* **2017**, *206*, 911–933. [CrossRef]
8. Zhang, C.; Zhao, T.; Xu, Q.; An, L.; Zhao, G. Effects of operating temperature on the performance of vanadium redox flow batteries. *Appl. Energy* **2015**, *155*, 349–353. [CrossRef]
9. Rana, M.M.; Uddin, M.; Sarkar, M.R.; Shafiullah, G.; Mo, H.; Atef, M. A review on hybrid photovoltaic–Battery energy storage system: Current status, challenges, and future directions. *J. Energy Storage* **2022**, *51*, 104597. [CrossRef]
10. Zhou, P.; Jin, R.Y.; Fan, L.W. Reliability and economic evaluation of power system with renewables: A review. *Renew. Sustain. Energy Rev.* **2016**, *58*, 537–547. [CrossRef]
11. Shafiullah, G.M.; Arif, M.T.; Oo, A.M.T. Mitigation strategies to minimize potential technical challenges of renewable energy integration. *Sustain. Energy Technol. Assess.* **2018**, *25*, 24–42. [CrossRef]
12. Babacan, O.; Torre, W.; Kleissl, J. Siting and sizing of distributed energy storage to mitigate voltage impact by solar PV in distribution systems. *Sol. Energy* **2017**, *146*, 199–208. [CrossRef]
13. Das, C.K.; Bass, O.; Mahmoud, T.S.; Kothapalli, G.; Mousavi, N.; Habibi, D.; Masoum, M.A. Optimal allocation of distributed energy storage systems to improve performance and power quality of distribution networks. *Appl. Energy* **2019**, *252*, 113468. [CrossRef]

14. Das, C.K.; Bass, O.; Kothapalli, G.; Mahmoud, T.S.; Habibi, D. Optimal placement of distributed energy storage systems in distribution networks using artificial bee colony algorithm. *Appl. Energy* **2018**, *232*, 212–228. [CrossRef]
15. Kalkhambkar, V.; Kumar, R.; Bhakar, R. Methodology for joint allocation of energy storage and renewable distributed generation. In Proceedings of the 2016 International Conference on Recent Advances and Innovations in Engineering (ICRAIE), Jaipur, India, 23–25 December 2016; pp. 1–8.
16. Lei, J.; Gong, Q. Operating strategy and optimal allocation of large-scale VRB energy storage system in active distribution networks for solar/wind power applications. *IET Gener. Transm. Distrib.* **2017**, *11*, 2403–2411. [CrossRef]
17. Nick, M.; Cherkaoui, R.; Paolone, M. Optimal planning of distributed energy storage systems in active distribution networks embedding grid reconfiguration. *IEEE Trans. Power Syst.* **2017**, *33*, 1577–1590. [CrossRef]
18. Mehmood, K.K.; Khan, S.U.; Lee, S.-J.; Haider, Z.M.; Rafique, M.K.; Kim, C.-H. Optimal sizing and allocation of battery energy storage systems with wind and solar power DGs in a distribution network for voltage regulation considering the lifespan of batteries. *IET Renew. Power Gener.* **2017**, *11*, 1305–1315. [CrossRef]
19. Taskforce, E.T. DER Roadmap. December 2019; p. 77. Available online: https://www.wa.gov.au/system/files/2020-04/DER_Roadmap.pdf (accessed on 15 June 2023).
20. Yang, M.; Chen, C.; Que, B.; Zhou, Z.; Yang, Q. Optimal placement and configuration of hybrid energy storage system in power distribution networks with distributed photovoltaic sources. In Proceedings of the 2018 2nd IEEE Conference on Energy Internet and Energy System Integration (EI2), Beijing, China, 20–22 October 2018; pp. 1–6.
21. Yan, N.; Zhang, B.; Li, W.; Ma, S. Hybrid energy storage capacity allocation method for active distribution network considering demand side response. *IEEE Trans. Appl. Supercond.* **2018**, *29*, 1–4. [CrossRef]
22. Awad, A.S.; El-Fouly, T.H.; Salama, M.M. Optimal ESS allocation and load shedding for improving distribution system reliability. *IEEE Trans. Smart Grid* **2014**, *5*, 2339–2349. [CrossRef]
23. Saboori, H.; Hemmati, R.; Jirdehi, M.A. Reliability improvement in radial electrical distribution network by optimal planning of energy storage systems. *Energy* **2015**, *93*, 2299–2312. [CrossRef]
24. Moradijoz, M.; Moghaddam, M.P.; Haghifam, M. A flexible active distribution system expansion planning model: A risk-based approach. *Energy* **2018**, *145*, 442–457. [CrossRef]
25. Murali, G.; Manivannan, A. Analysis of power quality problems in solar power distribution system. *Int. J. Eng. Res. Appl.* **2013**, *3*, 799–805.
26. Abdeltawab, H.; Mohamed, Y.A.-R.I. Mobile Energy Storage Sizing and Allocation for Multi-Services in Power Distribution Systems. *IEEE Access* **2019**, *7*, 176613–176623. [CrossRef]
27. Lei, J.; Gong, Q.; Liu, J.; Qiao, H.; Wang, B. Optimal allocation of a VRB energy storage system for wind power applications considering the dynamic efficiency and life of VRB in active distribution networks. *IET Renew. Power Gener.* **2019**, *13*, 563–571. [CrossRef]
28. Li, W.; Lu, C.; Pan, X.; Song, J. Optimal placement and capacity allocation of distributed energy storage devices in distribution networks. In Proceedings of the 2017 13th IEEE Conference on Automation Science and Engineering (CASE), Xi'an, China, 20–23 August 2017; pp. 1403–1407.
29. Wang, S.; Wang, K.; Teng, F.; Strbac, G.; Wu, L. Optimal allocation of ESSs for mitigating fluctuation in active distribution network. *Energy Procedia* **2017**, *142*, 3572–3577. [CrossRef]
30. Kim, I. Optimal capacity of storage systems and photovoltaic systems able to control reactive power using the sensitivity analysis method. *Energy* **2018**, *150*, 642–652. [CrossRef]
31. Ghatak, S.R.; Sannigrahi, S.; Acharjee, P. Multi-objective approach for strategic incorporation of solar energy source, battery storage system, and DSTATCOM in a smart grid environment. *IEEE Syst. J.* **2018**, *13*, 3038–3049. [CrossRef]
32. Li, B.; Li, X.; Bai, X.; Li, Z. Storage capacity allocation strategy for distribution network with distributed photovoltaic generators. *J. Mod. Power Syst. Clean Energy* **2018**, *6*, 1234–1243. [CrossRef]
33. Ahmed, H.M.; Awad, A.S.; Ahmed, M.H.; Salama, M. Mitigating voltage-sag and voltage-deviation problems in distribution networks using battery energy storage systems. *Electr. Power Syst. Res.* **2020**, *184*, 106294. [CrossRef]
34. Carpinelli, G.; Mottola, F.; Noce, C.; Russo, A.; Varilone, P. A new hybrid approach using the simultaneous perturbation stochastic approximation method for the optimal allocation of electrical energy storage systems. *Energies* **2018**, *11*, 1505. [CrossRef]
35. Wen, S.; Lan, H.; Fu, Q.; Yu, D.C.; Hong, Y.-Y.; Cheng, P. Optimal allocation of energy storage system considering multi-correlated wind farms. *Energies* **2017**, *10*, 625. [CrossRef]
36. Aming, D.; Rajapakse, A.; Molinski, T.; Innes, E. A technique for evaluating the reliability improvement due to energy storage systems. In Proceedings of the 2007 Canadian Conference on Electrical and Computer Engineering, Vancouver, BC, Canada, 22–26 April 2007; pp. 413–416.
37. Zhang, D.; Das, C.K.; Shafiullah, G.; Wong, K.W. Optimal allocation of distributed energy storage systems in unbalanced distribution networks. In Proceedings of the 2021 IEEE Asia-Pacific Conference on Computer Science and Data Engineering (CSDE), Brisbane, Australia, 8–10 December 2021; pp. 1–6.
38. Wang, S.; Luo, F.; Dong, Z.Y.; Ranzi, G. Joint planning of active distribution networks considering renewable power uncertainty. *Int. J. Electr. Power Energy Syst.* **2019**, *110*, 696–704. [CrossRef]
39. Ghiasi, M.; Ghadimi, N.; Ahmadinia, E. An analytical methodology for reliability assessment and failure analysis in distributed power system. *SN Appl. Sci.* **2019**, *1*, 44. [CrossRef]

40. Shoeb, M.A.; Shahnia, F.; Shafiullah, G. A multilayer and event-triggered voltage and frequency management technique for microgrid's central controller considering operational and sustainability aspects. *IEEE Trans. Smart Grid* **2018**, *10*, 5136–5151. [CrossRef]
41. Albadi, M.H.; Al Hinai, A.S.; Al-Badi, A.H.; Al Riyami, M.S.; Al Hinai, S.M.; Al Abri, R.S. Unbalance in power systems: Case study. In Proceedings of the 2015 IEEE International Conference on Industrial Technology (ICIT), Seville, Spain, 17–19 March 2015; pp. 1407–1411.
42. Ma, K.; Fang, L.; Kong, W. Review of distribution network phase unbalance: Scale, causes, consequences, solutions, and future research directions. *CSEE J. Power Energy Syst.* **2020**, *6*, 479–488.
43. Meersman, B.; Renders, B.; Degroote, L.; Vandoorn, T.; Vandevelde, L. Three-phase inverter-connected DG-units and voltage unbalance. *Electr. Power Syst. Res.* **2011**, *81*, 899–906. [CrossRef]
44. Das, C.K.; Bass, O.; Mahmoud, T.S.; Kothapalli, G.; Masoum, M.A.; Mousavi, N. An optimal allocation and sizing strategy of distributed energy storage systems to improve performance of distribution networks. *J. Energy Storage* **2019**, *26*, 100847. [CrossRef]
45. Mohsen, M.; Youssef, A.-R.; Ebeed, M.; Kamel, S. Optimal planning of renewable distributed generation in distribution systems using grey wolf optimizer GWO. In Proceedings of the 2017 Nineteenth International Middle East Power Systems Conference (MEPCON), Cairo, Egypt, 19–21 December 2017; pp. 915–921.
46. Ansari, M.M.; Guo, C.; Shaikh, M.S.; Chopra, N.; Haq, I.; Shen, L. Planning for distribution system with grey wolf optimization method. *J. Electr. Eng. Technol.* **2020**, *15*, 1485–1499. [CrossRef]
47. Goli, P.; Yelem, S.; Muaddi, S.; Gampa, S.R.; Shireen, W. Optimal Planning of Smart Charging Facilities using Grey Wolf Optimizer. In Proceedings of the 2022 IEEE Texas Power and Energy Conference (TPEC), College Station, TX, USA, 28 February–1 March 2022; pp. 1–6.
48. Sultana, U.; Khairuddin, A.B.; Mokhtar, A.; Zareen, N.; Sultana, B. Grey wolf optimizer based placement and sizing of multiple distributed generation in the distribution system. *Energy* **2016**, *111*, 525–536. [CrossRef]
49. Ikeda, S.; Ooka, R. Metaheuristic optimization methods for a comprehensive operating schedule of battery, thermal energy storage, and heat source in a building energy system. *Appl. Energy* **2015**, *151*, 192–205. [CrossRef]
50. Koad, R.B.; Zobaa, A.F.; El-Shahat, A. A novel MPPT algorithm based on particle swarm optimization for photovoltaic systems. *IEEE Trans. Sustain. Energy* **2016**, *8*, 468–476. [CrossRef]
51. Allan, R.N.; Billinton, R.; Sjarief, I.; Goel, L.; So, K. A reliability test system for educational purposes-basic distribution system data and results. *IEEE Trans. Power Syst.* **1991**, *6*, 813–820. [CrossRef]
52. Billinton, R.; Allan, R.N. *Reliability Evaluation of Power Systems*; Springer Science & Business Media: Berlin/Heidelberg, Germany, 2013.
53. Adefarati, T.; Bansal, R. Integration of renewable distributed generators into the distribution system: A review. *IET Renew. Power Gener.* **2016**, *10*, 873–884. [CrossRef]
54. Adefarati, T.; Bansal, R. Reliability assessment of distribution system with the integration of renewable distributed generation. *Appl. Energy* **2017**, *185*, 158–171. [CrossRef]
55. Nojavan, S.; Zare, K. *Demand Response Application in Smart Grid*; Springer: Berlin/Heidelberg, Germany, 2020.
56. *IEEE Guide for Electric Power Distribution Reliability Indices*; IEEE: Piscataway, NJ, USA, 2012; pp. 1–43.
57. Jayasekara, N.; Masoum, M.A.; Wolfs, P.J. Optimal operation of distributed energy storage systems to improve distribution network load and generation hosting capability. *IEEE Trans. Sustain. Energy* **2015**, *7*, 250–261. [CrossRef]
58. Zhong, S.; Qiu, J.; Sun, L.; Liu, Y.; Zhang, C.; Wang, G. Coordinated planning of distributed WT, shared BESS and individual VESS using a two-stage approach. *Int. J. Electr. Power Energy Syst.* **2020**, *114*, 105380. [CrossRef]
59. Bloomberg Finance. Behind the Scenes Take on Lithium-ion Battery Prices. 2019. Available online: https://about.bnef.com/blog/behind-scenes-take-lithium-ion-battery-prices (accessed on 22 June 2023).
60. Valøen, L.O.; Shoesmith, M.I. The effect of PHEV and HEV duty cycles on battery and battery pack performance. In Proceedings of the PHEV 2007 Conference, Winnipeg, MB, Canada, 1–2 November 2007; pp. 4–5.
61. Frankel, D.; Kane, S.; Tryggestad, C. The New Rules of Competition in Energy Storage. 2018. Available online: https://www.mckinsey.com/ (accessed on 20 June 2023).
62. Asenbauer, J.; Eisenmann, T.; Kuenzel, M.; Kazzazi, A.; Chen, Z.; Bresser, D. The success story of graphite as a lithium-ion anode material–fundamentals, remaining challenges, and recent developments including silicon (oxide) composites. *Sustain. Energy Fuels* **2020**, *4*, 5387–5416. [CrossRef]
63. Hornsdale Power Reserve. Available online: https://hornsdalepowerreserve.com.au/?sfw=pass1619474757 (accessed on 18 June 2023).
64. Jabr, R.A.; Džafić, I.; Pal, B.C. Robust optimization of storage investment on transmission networks. *IEEE Trans. Power Syst.* **2014**, *30*, 531–539. [CrossRef]
65. Luo, K. Enhanced grey wolf optimizer with a model for dynamically estimating the location of the prey. *Appl. Soft Comput.* **2019**, *77*, 225–235. [CrossRef]
66. Mirjalili, S.; Mirjalili, S.M.; Lewis, A. Grey wolf optimizer. *Adv. Eng. Softw.* **2014**, *69*, 46–61. [CrossRef]
67. Baran, M.E.; Wu, F.F. Network reconfiguration in distribution systems for loss reduction and load balancing. *IEEE Trans. Power Deliv.* **1989**, *4*, 1401–1407. [CrossRef]
68. Swarnkar, A.; Gupta, N.; Niazi, K.R. Adapted ant colony optimization for efficient reconfiguration of balanced and unbalanced distribution systems for loss minimization. *Swarm Evol. Comput.* **2011**, *1*, 129–137. [CrossRef]

69. Power, W. Technical Rules December. 2016. Available online: https://www.westernpower.com.au/media/2312/technical-rules-20161201.pdf (accessed on 16 June 2023).
70. Sereeter, B.; Vuik, K.; Witteveen, C. Newton Power Flow Methods for Unbalanced Three-Phase Distribution Networks. *Energies* **2017**, *10*, 1658. [CrossRef]
71. Kumawat, M.; Gupta, N.; Jain, N.; Bansal, R.C. Swarm-Intelligence-Based Optimal Planning of Distributed Generators in Distribution Network for Minimizing Energy Loss. *Electr. Power Compon. Syst.* **2017**, *45*, 589–600. [CrossRef]
72. Qiu, J.; Xu, Z.; Zheng, Y.; Wang, D.; Dong, Z.Y. Distributed generation and energy storage system planning for a distribution system operator. *IET Renew. Power Gener.* **2018**, *12*, 1345–1353. [CrossRef]
73. Zhang, M.; Gan, M.; Li, L. Sizing and siting of distributed generators and energy storage in a microgrid considering plug-in electric vehicles. *Energies* **2019**, *12*, 2293. [CrossRef]
74. Mukhopadhyay, B.; Das, D. Multi-objective dynamic and static reconfiguration with optimized allocation of PV-DG and battery energy storage system. *Renew. Sustain. Energy Rev.* **2020**, *124*, 109777. [CrossRef]
75. Saboori, H.; Hemmati, R. Maximizing DISCO profit in active distribution networks by optimal planning of energy storage systems and distributed generators. *Renew. Sustain. Energy Rev.* **2017**, *71*, 365–372. [CrossRef]
76. Karaboga, D.; Akay, B. A comparative study of artificial bee colony algorithm. *Appl. Math. Comput.* **2009**, *214*, 108–132. [CrossRef]
77. Kennedy, J.; Eberhart, R. Particle swarm optimization. In Proceedings of the ICNN'95-International Conference on Neural Networks, Perth, Australia, 27 November–1 December 1995; pp. 1942–1948.
78. Chopard, B.; Tomassini, M. Particle swarm optimization. In *An Introduction to Metaheuristics for Optimization*; Springer: Berlin/Heidelberg, Germany, 2018; pp. 97–102.